

# The Cosmic Organism Theory of Physics: changeable universes and physical laws

## Principles

*The Object Structure*

$$3_{11}, 2_{10}, 1_{4to10}, 0_4 \text{ to } 11$$

*The Space Structure*

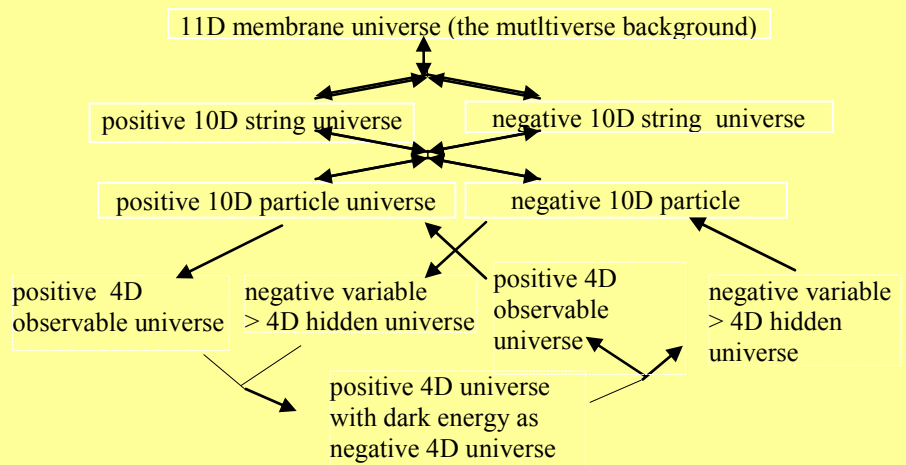
$$(1)_n + (0)_n \xrightarrow{\text{combination}}$$

$$(10)_n, (1+0)_n, \text{ or } (1)_n(0)_n$$

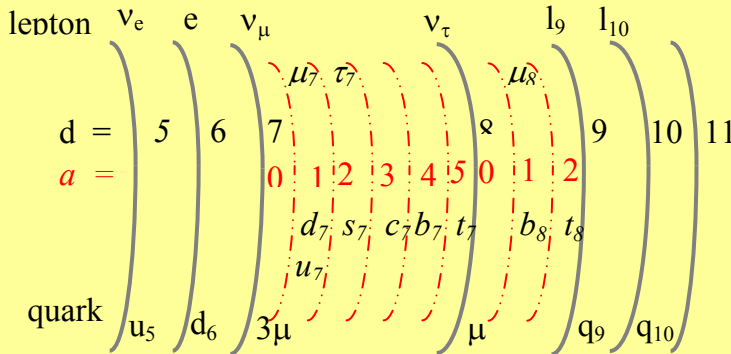
*The Dimensional Oscillation*

$$E = M c^2 / \alpha^{2(D-4)}$$

## Cosmology



## Elementary Particles



## Extreme Force

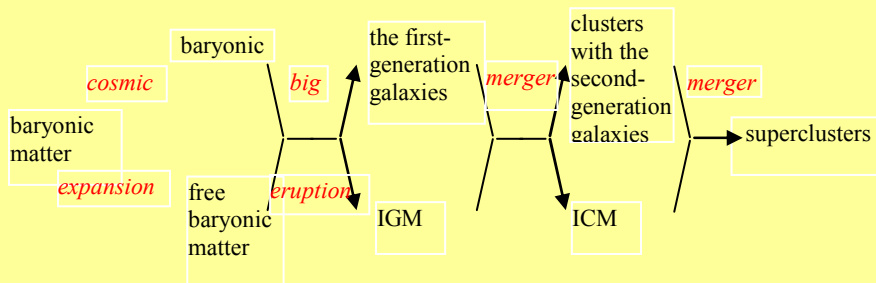
$$\binom{1_4}{4}_m + \sum_{k=1}^k \left( \binom{0_4}{4} \binom{1_4}{4} \right)_{n,k} \xrightarrow{\text{extreme condition}}$$

particle gauge boson field in binary lattice space

$$\binom{1_4}{4}_m + \sum_{k=1}^k \binom{0_4}{4}_{n,k} \binom{1_4}{4}_{n,k}$$

extreme particle extreme boson field in binary partition space

## Galaxies



# The Cosmic Organism Theory of Physics: changeable universes and physical laws

## Contents

<b>Abstract</b>	3
<b>1 The Three Physical Principles</b>	
Introduction	4
1.1 The Object Structure	4
1.2 The Space Structure	4
1.3 The Dimensional Oscillation	7
1.4 Summary	9
<b>2 Cosmology</b>	
Introduction	10
2.1. The Strong Universe	10
2.2. The Gravitational Universe	10
2.3. The Charged Universe	11
2.4. The Current Universe	13
2.5. The Periodic Table of Elementary Particles	23
2.5.1. The CP Asymmetry	23
2.5.2. The Boson Mass Formula	24
2.5.3. The Mass Composites of Leptons and Quarks	26
2.5.4. The Lepton Mass Formula	28
2.5.5. The Quark Mass Formula	29
2.6. Summary	30
<b>3 The Galaxy Formation</b>	
Introduction	31
3.1 The Separation between Baryonic Matter and Dark Matter	31
3.2 The Formation of the Inhomogeneous Structures	34
3.3 Summary	41
<b>4 Extreme Force Field</b>	
4.1. The quantum space phase transitions for force fields	43
4.2. Superconductor and the Fractional Quantum Hall Effect	44
4.3. Gravastar, Supernova, Neutron Star, and GRB	49
4.4. Summary	57
<b>5 Summary</b>	58
<b>6 Reference</b>	59

## Abstract

In the cosmic organism theory of physics, the universes and the physical laws are changeable, and they are the variable expressions of the cosmic code, as the biological organs of an organism are the variable expressions of the genetic code. The cosmic organism of physics is the theory of everything to explain fully cosmology, dark energy, dark matter, baryonic matter, quantum mechanics, elementary particles, force fields, galaxy formation, and unusual extreme forces. The cosmic organism theory is divided into five parts: the three physical principles, cosmology, the periodic table of elementary particles, the galaxy formation, and the extreme force field. The cosmic code consists of the three physical principles: the object structure, the space structure, and the dimensional oscillation. The object structure consists of 11D membrane ( $3_{11}$ ), 10D string ( $2_{10}$ ), variable D particle ( $1_{\leq 10}$ ), and empty object (0). The space structure includes attachment space (1) and detachment space (0). Relating to rest mass, attachment space attaches to object permanently with zero speed or reversibly at the speed of light. Relating to kinetic energy, detachment space irreversibly detaches from the object at the speed of light. The combination of attachment space and detachment space brings about three different space structures: miscible space, binary lattice space, and binary partition space for special relativity, quantum mechanics, and the extreme force fields, respectively. The dimensional oscillation involves the oscillation between high dimensional space-time with high vacuum energy and low dimensional space-time with low vacuum energy. Our observable universe with 4D space-time has zero vacuum energy.

In terms of cosmology, our universe starts with the 11-dimensional membrane universe followed by the 10-dimensional string universe and then by the 10-dimensional particle universe, and ends with the asymmetrical dual universe with variable dimensional particle and 4-dimensional particles. Such 4-stage cosmology accounts for the origins of the four force fields. The unified theory places all elementary particles in the periodic table of elementary particles with the calculated masses in good agreement with the observed values.

The inhomogeneous structures, such as galaxy, is derived from the incompatibility between baryonic matter and dark matter, like the inhomogeneous structure formed by the incompatibility between oil and water. Cosmic radiation allows dark matter and baryonic matter to be compatible. As the universe expanded, the decreasing density of cosmic radiation increased the incompatibility, resulting in increasing inhomogeneous structures. The five stages of the formation of inhomogeneous structures are baryonic matter, baryonic droplets, the first generation galaxies by the big eruption, cluster, and supercluster. The big eruption explains the origin of different types of galaxies.

Under extreme conditions, such as the zero temperature and extremely high pressure, gauge boson force field undergoes the phase transition to form extreme force field. Extreme force field explains unusual phenomena such as superconductor, fractional quantum Hall effect, supernova, neutron star, gamma ray burst, and quasar.

# 1. The Three Physical Principles

## Introduction

Our observable universe is a complex universe. It has at least four force fields; the strong, the gravitational, the electromagnetic (charged), and the weak force fields. It has at least four different materials and energies: cosmic radiation, dark energy, dark matter, and baryonic matter. It has numerous elementary particles, including six leptons, six quarks, and gauge bosons. So far, there is no viable unified theory in physics to unify specifically all these different phenomena.

The unified theory of physics unifies various phenomena in our observable universe and other universes. The unified theory of physics is derived from the cosmic organism theory [1] [2]. In the cosmic organism theory, all universes are governed by the cosmic code, like genetic code. Different universes with different physical laws are the different expressions of the same cosmic code, as different organs in an organism are different gene expressions of the same genetic code. The cosmic organism theory is divided into five parts: the three physical principles, cosmology, the periodic table of elementary particles, the galaxy formation, and the extreme force field. The cosmic code consists of three parts as the three physical principles: the object structure, the space structure, and the dimensional oscillation.

### 1.1. The Object Structure

The first part of the physical principles is the object structure. The object structure consists of 11D membrane ( $3_{11}$ ), 10D string ( $2_{10}$ ), variable D particle ( $1_{4 \text{ to } 10}$ ), and empty object (0). Different universes and different stages of a universe can have different expressions of the object structure. For an example, the four stages in the evolution of our universe are the 11D membrane universe (the strong universe), the dual 10D string universe (the gravitational pre-universe), the dual 10D particle universe (the charged pre-universe), and the dual 4D/variable D particle universe (the current universe).

### 1.2. The Space Structure

The second part of the physical principles is the space structure. The space structure [3] [4] consists of attachment space (denoted as 1) and detachment space (denoted as 0). Attachment space attaches to object permanently with zero speed or reversibly at the speed of light. Detachment space irreversibly detaches from the object at the speed of light. Attachment space relates to rest mass, while detachment space relates to kinetic energy. Different stages of our universe have different space structures.

The cosmic origin of detachment space is the cosmic radiation from the particle-antiparticle annihilation that initiates the inflation as shown later. Some objects in 4D-attachment space, denoted as  $1_4$ , convert into the cosmic radiation in 4D-detachment space, denoted as  $0_4$ . Cosmic radiation cannot permanently attach to a space.

$$\text{some objects in } 1_4 \longrightarrow \text{the cosmic radiation in } 0_4 \quad (1)$$

The combination of attachment space (1) and detachment space (0) brings about three different space structures: miscible space, binary partition space, and binary lattice space for four-dimensional space-time as below.

$$(1)_n \text{ attachment space} + (0)_n \text{ detachment space} \xrightarrow{\text{combination}} \quad (2)$$

$$(10)_n \text{ binary lattice space, } (1+0)_n \text{ miscible space, or } (1)_n(0)_n \text{ binary partition space}$$

Binary lattice space,  $(10)_n$ , consists of repetitive units of alternative attachment space and detachment space. Thus, binary lattice space consists of multiple quantized units of attachment space separated from one another by detachment space. In miscible space, attachment space is miscible to detachment space, and there is no separation of attachment space and detachment space. Binary partition space,  $(1)_n(0)_n$ , consists of separated continuous phases of attachment space and detachment space.

Binary lattice space consists of multiple quantized units of attachment space separated from one another by detachment space. An object exists in multiple quantum states separated from one another by detachment space. Binary lattice space is the space for wavefunction. In wavefunction,

$$|\Psi\rangle = \sum_{i=1}^n c_i |\phi_i\rangle \quad , \quad (3)$$

Each individual basis element,  $|\phi_i\rangle$ , attaches to attachment space, and separates from the adjacent basis element by detachment space. Detachment space detaches from object. Binary lattice space with n units of four-dimensional,  $(01)_n$ , contains n units of basis elements.

Neither attachment space nor detachment space is zero in binary lattice space. The measurement in the uncertainty principle in quantum mechanics is essentially the measurement of attachment space and momentum in binary lattice space: large momentum has small non-zero attachment space, while large attachment space has low non-zero momentum. In binary lattice space, an entity is both in constant motions as wave for detachment space and in stationary state as a particle for attachment space, resulting in the wave-particle duality.

Detachment space contains no object that carries information. Without information, detachment space is outside of the realm of causality. Without causality, distance (space) and time do not matter to detachment space, resulting in non-localizable and non-countable space-time. The requirement for the system (binary lattice space) containing non-localizable and non-countable detachment space is the absence of net information by any change in the space-time of detachment space. All changes have to be coordinated to result in zero net information. This coordinated non-localized binary lattice space corresponds to nilpotent space. All changes in energy, momentum, mass,

time, space have to result in zero as defined by the generalized nilpotent Dirac equation by B. M. Diaz and P. Rowlands [5].

$$(\mp \mathbf{k} \partial / \partial t \pm \mathbf{i} \nabla + \mathbf{j} m)(\pm i \mathbf{k} E \pm \mathbf{i} \mathbf{p} + \mathbf{j} m) \exp i(-Et + \mathbf{p} \cdot \mathbf{r}) = 0 \quad , \quad (4)$$

where  $E$ ,  $\mathbf{p}$ ,  $m$ ,  $t$  and  $\mathbf{r}$  are respectively energy, momentum, mass, time, space and the symbols  $\pm 1$ ,  $\pm i$ ,  $\pm \mathbf{i}$ ,  $\pm \mathbf{j}$ ,  $\pm \mathbf{k}$ ,  $\pm \mathbf{i}$ ,  $\pm \mathbf{j}$ ,  $\pm \mathbf{k}$ , are used to represent the respective units required by the scalar, pseudoscalar, quaternion and multivariate vector groups. The changes involve the sequential iterative path from nothing (nilpotent) through conjugation, complexification, and dimensionalization. The non-local property of binary lattice space for wavefunction provides the violation of Bell inequalities [6] in quantum mechanics in terms of faster-than-light influence and indefinite property before measurement. The non-locality in Bell inequalities does not result in net new information.

In binary lattice space, for every detachment space, there is its corresponding adjacent attachment space. Thus, no part of the object can be irreversibly separated from binary lattice space, and no part of a different object can be incorporated in binary lattice space. Binary lattice space represents coherence as wavefunction. Binary lattice space is for coherent system. Any destruction of the coherence by the addition of a different object to the object causes the collapse of binary lattice space into miscible space. The collapse is a phase transition from binary lattice space to miscible space.

$$\begin{array}{ccc} ((0)(1))_n & \xrightarrow{\text{collapse}} & (0+1)_n \\ \text{binary lattice space} & & \text{miscible space} \end{array} \quad (5)$$

Another way to convert binary lattice space into miscible space is gravity. Penrose [7] pointed out that the gravity of a small object is not strong enough to pull different states into one location. On the other hand, the gravity of large object pulls different quantum states into one location to become miscible space. Therefore, a small object without outside interference is always in binary lattice space, while a large object is never in binary lattice space.

The information in miscible space is contributed by the combination of both attachment space and detachment space, so information can no longer be non-localize. Any value in miscible space is definite. All observations in terms of measurements bring about the collapse of wavefunction, resulting in miscible space that leads to eigenvalue as definite quantized value. Such collapse corresponds to the appearance of eigenvalue,  $E$ , by a measurement operator,  $H$ , on a wavefunction,  $\Psi$ .

$$H \Psi = E \Psi \quad , \quad (6)$$

In miscible space, attachment space is miscible to detachment space, and there is no separation of attachment space and detachment space. In miscible space, attachment space contributes zero speed, while detachment space contributes the speed of light. A massless particle, such as photon, is on detachment space continuously, and detaches from its own space continuously. For a moving massive particle consisting of a rest massive part and a massless part, the massive part with rest mass,  $m_0$ , is in attachment space, and the

massless part with kinetic energy,  $K$ , is in detachment space. The combination of the massive part in attachment space and massless part in detachment leads to the propagation speed in between zero and the speed of light.

To maintain the speed of light constant for a moving particle, the time ( $t$ ) in moving particle has to be dilated, and the length ( $L$ ) has to be contracted relative to the rest frame.

$$\begin{aligned}
 t &= t_0 / \sqrt{1 - v^2 / c^2} = t_0 \gamma, \\
 L &= L_0 / \gamma, \\
 E &= K + m_0 c^2 = \gamma m_0 c^2
 \end{aligned}
 \tag{7}$$

where  $\gamma = 1 / \sqrt{1 - v^2 / c^2}$  is the Lorentz factor for time dilation and length contraction,  $E$  is the total energy and  $K$  is the kinetic energy.

Binary partition space,  $(1)_n(0)_n$ , consists of separated continuous phases of attachment space and detachment space. It is for extreme force fields under extreme conditions such as near the absolute zero temperature or extremely high pressure. It will be discussed later to explain extreme phenomena such as superconductivity and black hole.

### 1.3. The Dimensional Oscillation

The third part of the physical principles is the dimensional oscillation [2]. The dimensional oscillation involves the oscillation between high dimensional space-time and low dimensional space-time. The vacuum energy of the multiverse background is about the Planck energy. Vacuum energy decreases with decreasing dimension number. The vacuum energy of 4D space-time is zero. With such vacuum energy differences, the local dimensional oscillation between high and low space-time dimensions results in local eternal expansion-contraction [8] [9] [10]. Eternal expansion-contraction is like harmonic oscillator, oscillating between the Planck vacuum energy and the lower vacuum energy.

For the dimensional oscillation, contraction occurs at the end of expansion. Each local region in the universe follows a particular path of the dimensional oscillation. Each path is marked by particular set of force fields. The path for our universe is marked by the strong force, gravity-antigravity, charged electromagnetism, and asymmetrical weak force, corresponding to the four stages of the cosmic evolution.

The vacuum energy differences among space-time dimensions are based on the varying speed of light. Varying speed of light has been proposed to explain the horizon problem of cosmology [11][12]. The proposal is that light traveled much faster in the distant past to allow distant regions of the expanding universe to interact since the beginning of the universe. Therefore, it was proposed as an alternative to cosmic inflation. J. D. Barrow [13] proposes that the time dependent speed of light varies as some power of the expansion scale factor  $a$  in such way that

$$c(t) = c_0 a^n \tag{8}$$

where  $c_0 > 0$  and  $n$  are constants. The increase of speed of light is continuous.

In this paper, varying dimension number (VDN) relates to quantized varying speed of light (QVSL), where the speed of light is invariant in a constant space-time dimension number, and the speed of light varies with varying space-time dimension number from 4 to 11.

$$c_D = c / \alpha^{D-4}, \quad (9)$$

where  $c$  is the observed speed of light in the 4D space-time,  $c_D$  is the quantized varying speed of light in space-time dimension number,  $D$ , from 4 to 11, and  $\alpha$  is the fine structure constant for electromagnetism. Each dimensional space-time has a specific speed of light. (Since from the beginning of our observable universe, the space-time dimension has always been four, there is no observable varying speed of light in our observable universe.) The speed of light increases with the increasing space-time dimension number  $D$ .

In special relativity,  $E = M_0 c^2$  modified by Eq. (9) is expressed as

$$E = M_0 \cdot (c^2 / \alpha^{2(D-4)}) \quad (10a)$$

$$= (M_0 / \alpha^{2(d-4)}) \cdot c^2. \quad (10b)$$

Eq. (10a) means that a particle in the  $D$  dimensional space-time can have the superluminal speed  $c / \alpha^{D-4}$ , which is higher than the observed speed of light  $c$ , and has the rest mass  $M_0$ . Eq. (10b) means that the same particle in the 4D space-time with the observed speed of light acquires  $M_0 / \alpha^{2(d-4)}$  as the rest mass, where  $d = D$ .  $D$  in Eq. (10a) is the space-time dimension number defining the varying speed of light. In Eq. (10b),  $d$  from 4 to 11 is “mass dimension number” defining varying mass. For example, for  $D = 11$ , Eq. (10a) shows a superluminal particle in eleven-dimensional space-time, while Eq. (10b) shows that the speed of light of the same particle is the observed speed of light with the 4D space-time, and the mass dimension is eleven. In other words, 11D space-time can transform into 4D space-time with 11d mass dimension. 11D4d in Eq. (10a) becomes 4D11d in Eq. (10b) through QVSL. QVSL in terms of varying space-time dimension number,  $D$ , brings about varying mass in terms of varying mass dimension number,  $d$ .

The QVSL transformation transforms both space-time dimension number and mass dimension number. In the QVSL transformation, the decrease in the speed of light leads to the decrease in space-time dimension number and the increase of mass in terms of increasing mass dimension number from 4 to 11,

$$c_D = c_{D-n} / \alpha^{2n}, \quad (11a)$$

$$M_{0,D,d} = M_{0,D-n,d+n} \alpha^{2n}, \quad (11b)$$

$$D, d \xrightarrow{QVSL} (D \mp n), (d \pm n) \quad (11c)$$

where  $D$  is the space-time dimension number from 4 to 11 and  $d$  is the mass dimension number from 4 to 11. For example, in the QVSL transformation, a particle with 11D4d is

transformed to a particle with 4D11d. In terms of rest mass, 11D space-time has 4d with the lowest rest mass, and 4D space-time has 11d with the highest rest mass.

Rest mass decreases with increasing space-time dimension number. The decrease in rest mass means the increase in vacuum energy, so vacuum energy increases with increasing space-time dimension number. The vacuum energy of 4D particle is zero, while 11D membrane has the Planck vacuum energy. Such vacuum energies are the alternatives for the Higgs bosons, which have not been found. The decrease in vacuum energy is equivalent to the absorption of the Higgs boson, while the increase in vacuum energy is equivalent to the emission of the Higgs boson.

Since the speed of light for  $> 4D$  particle is greater than the speed of light for 4D particle, the observation of  $> 4D$  particles by 4D particles violates casualty. Thus,  $> 4D$  particles are hidden particles with respect to 4D particles. Particles with different space-time dimensions are transparent and oblivious to one another, and separate from one another if possible.

#### **1.4. Summary**

The unified theory of physics is derived from the cosmic organism theory. In the cosmic organism theory, different universes are the different expressions of the same cosmic code, as different organs are the different genetic expressions of the same genetic code in an organism. The different universes constitute the cosmic organism in the cosmic organism theory that is the unified theory to unify various phenomena in our observable universe and in different universes. The cosmic code consists of the object structure, the space structure, and the dimensional oscillation. The object structure consists of 11D membrane ( $3_{11}$ ), 10D string ( $2_{10}$ ), variable D particle ( $1_{\leq 10}$ ), and empty object (0). The space structure includes attachment space (1) and detachment space (0). Relating to rest mass, attachment space attaches to object permanently with zero speed or reversibly at the speed of light. Relating to kinetic energy, detachment space irreversibly detaches from the object at the speed of light. In our observable universe, the space structure consists of three different combinations of attachment space and detachment space, describing three different phenomena: quantum mechanics, special relativity, and the extreme force fields. The dimensional oscillation involves the oscillation between high dimensional space-time with high vacuum energy and low dimensional space-time with low vacuum energy. Our observable universe with 4D space-time has zero vacuum energy.

## 2. Cosmology

### Introduction

Before the current universe, the pre-universe is in the three different stages in chronological order: the strong pre-universe, the gravitational pre-universe, and the charged pre-universe. The strong pre-universe has only one force: the strong force. The gravitational pre-universe has two forces: the strong and the gravitational forces. The charged pre-universe has three forces: the strong, the gravitational, and the electromagnetic forces. All three forces in the pre-universes are in their primitive forms unlike the finished forms in our observable universe. The asymmetrical weak interaction comes from the formation of the current asymmetrical dual universe. Such 4-stage cosmology for our universe explains the origin of the four force fields in our observable universe.

#### 2.1. The Strong Pre-Universe

Dual universe	Object structure	Space structure	Force
no	11D membrane	attachment space	pre-strong

Many different universes can emerge from the multiverse background, which has the simplest and most primitive structure [1] [2]. As in Einstein's static universe, the time in the multiverse background has no beginning. Different parts of the background have potential to undergo local inhomogeneity to develop different universes with different object structures, space structures, and vacuum energies. The multiverse background is the strong pre-universe. It is the homogeneous static universe, consisting of 11D (space-time dimensional) positive energy membrane and negative energy anti-membrane, denoted as  $3_{11} 3_{-11}$ , as proposed by Mongan [14]. The only force among the membranes is the pre-strong force,  $s$ , as the predecessor of the strong force. It is from the quantized vibration of the membranes to generate the reversible process of the absorption-emission of the massless particles among the membranes. The pre-strong force mediates the reversible absorption-emission in the flat space. The pre-strong force is the same for all membranes, so it is not defined by positive or negative sign. It does not have gravity that causes instability and singularity [15], so the initial universe remains homogeneous, flat, and static. This initial universe provides the globally stable static background state for an inhomogeneous eternal universe in which local regions undergo expansion-contraction [15].

#### 2.2. The Gravitational Pre-Universe

Dual universe	Object structure	Space structure	Forces
dual	10D string	attachment space	pre-strong, pre-gravity

In certain regions of the 11D membrane universe, the local expansion takes place by the transformation from 11D-membrane into 10D-string. The expansion is the result of the vacuum energy difference between 11D membrane and 10D string. With the

emergence of empty object ( $0_{11}$ ), 11D membrane transforms into 10D string warped with virtue particle as pregravity.

$$3_{11}s + 0_{11} \longleftrightarrow 2_{10}s1_1 = 2_{10}s g^+ \quad (12)$$

where  $3_{11}$  is the 11D membrane,  $s$  is the pre-strong force,  $0_{11}$  is the 11D empty object,  $2_{10}$  is 10D string,  $1_1$  is one dimensional virtue particle as  $g$ , pre-gravity. Empty object corresponds to the anti-De Sitter bulk space in the Randall-Sundrum model [16]. In the same way, the surrounding object can extend into empty object by the decomposition of space dimension as described by Bounias and Krasnoholovets [17], equivalent to the Randall-Sundrum model. The  $g$  is in the bulk space, which is the warped space (transverse radial space) around  $2_{10}$ . As in the AdS/CFT duality [18] [19] [20], the pre-strong force has 10D dimension, one dimension lower than the 11D membrane, and is the conformal force defined on the conformal boundary of the bulk space. The pre-strong force mediates the reversible absorption-emission process of membrane (string) units in the flat space, while pregravity mediates the reversible condensation-decomposition process of mass-energy in the bulk space.

Through symmetry, antistrings form 10D antibranes with anti-pregravity as  $2_{-10} g^-$ , where  $g^-$  is anti-pregravity.

$$3_{-11}s + 0_{-11} \longleftrightarrow 2_{-10}s 1_{-1} = 2_{-10}s g^- \quad (13)$$

Pregravity can be attractive or repulsive to anti-pregravity. If it is attractive, the universe remains homogeneous. If it is repulsive,  $n$  units of  $(2_{10})_n$  and  $n$  units of  $(2_{-10})_n$  are separated from each other.

$$((s2_{10})g^+)_n (g^-(s2_{-10}))_n \quad (14)$$

The universe with pregravity and anti-pregravity is the dual 10D string universe, which leads to the evolution of our observable universe. The dual 10D string universe consists of two parallel universes with opposite energies: 10D strings with positive energy and 10D antistrings with negative energy. The two universes are separated by the bulk space, consisting of pregravity and anti-pregravity. Such dual universe separated by bulk space appears in the ekpyrotic universe model [21] [22].

### 2.3. The Charged Pre-Universe

Dual universe	Object structure	Space structure	Forces
dual	10D particle	attachment space	pre-strong, pre-gravity, pre-electromagnetic

When the local expansion stops, through the dimensional oscillation, the contraction begins to force the dual 10D string universe to contract to the original state, resulting in the coalescence of the two universes. The coalescence allows the two universes to mix. The first path of such mixing is the string-antistring annihilation, resulting in disappearance of

the dual universe and the return to the multiverse background. The outcome is the completion of one oscillating cycle.

The second path allows the continuation of the dual universe in another form without the mixing of positive energy and negative energy. Such dual universe is possible by the emergence of the pre-charge force, the predecessor of electromagnetism with positive and negative charges. The mixing becomes the mixing of positive charge and negative charge instead of positive energy and negative energy, resulting in the preservation of the dual universe with the positive energy and the negative energy. Our universe follows the second path as described below in details.

During the coalescence for the second path, the two universes coexist in the same space-time, which is predicted by the Santilli isodual theory [23]. Antiparticle for our positive energy universe is described by Santilli as follows, “this identity is at the foundation of the perception that antiparticles “appear” to exist in our space, while in reality they belong to a structurally different space coexisting within our own, thus setting the foundations of a “multidimensional universe” coexisting in the same space of our sensory perception” (Ref. 23, p. 94). Antiparticles in the positive energy universe actually come from the coexisting negative energy universe.

The mixing process follows the isodual hole theory that is the combination of the Santilli isodual theory and the Dirac hole theory. In the Dirac hole theory that is not symmetrical, the positive energy observable universe has an unobservable infinitive sea of negative energy. A hole in the unobservable infinitive sea of negative energy is the observable positive energy antiparticle.

In the dual 10D string universe, one universe has positive energy strings with pregravity, and one universe has negative energy antistrings with anti-pregravity. For the mixing of the two universes during the coalescence, a new force, the pre-charged force, emerges to provide the additional distinction between string and antistring. The pre-charged force is the predecessor of electromagnetism. Before the mixing, the positive energy string has positive pre-charge ( $e^+$ ), while the negative energy antistring has negative pre-charge ( $e^-$ ). During the mixing when two 10D string universes coexist, a half of positive energy strings in the positive energy universe move to the negative energy universe, and leave the Dirac holes in the positive energy universe. The negative energy antistrings that move to fill the holes become positive energy antistrings with negative pre-charge in the positive energy universe. In terms of the Dirac hole theory, the unobservable infinitive sea of negative energy is in the negative energy universe from the perspective of the positive energy universe before the mixing. The hole is due to the move of the negative energy antistring to the positive energy universe from the perspective of the positive energy universe during the mixing, resulting in the positive energy antistring with negative pre-charge in the positive energy universe.

In the same way, a half of negative energy antistrings in the negative energy universe moves to the positive energy universe, and leave the holes in the negative energy universe. The positive energy strings that move to fill the holes become negative energy strings with positive pre-charge in the negative energy universe. The result of the mixing is that both positive energy universe and the negative energy universe have strings-antistrings. The existence of the pre-charge provides the distinction between string and antistring in the string-antistring.

At that time, the space (detachment space) for radiation has not appeared in the universe, so the string-antistring annihilation does not result in radiation. The string-antistring annihilation results in the replacement of the string-antistring as the 10D string-antistring,  $(2_{10} 2_{-10})$  by the 10D particle-antiparticle  $(1_{10} 1_{-10})$ . The 10D particles-antiparticles have the multiple dimensional Kaluza-Klein structure with variable space dimension number without the requirement for a fixed space dimension number for string-antistring. After the mixing, the dual 10D particle-antiparticle universe separated by pregravity and anti-pregravity appears as below.

$$((s1_{10} e^+ e^- 1_{-10} s)g^+)_n (g^-(s1_{10} e^+ e^- 1_{-10} s))_n, \quad (15)$$

where  $s$  and  $e$  are the pre-strong force and the pre-charged force in the flat space,  $g$  is pregravity in the bulk space, and  $1_{10} 1_{-10}$  is the particle-antiparticle. The dual 10D particle universe has particles, while the multiverse background (11D- membrane universe) has membranes, so the multiverse background and the dual 10D particle universe are completely transparent and oblivious to each other. The result is the free charged dual 10D particle-antiparticle universe.

The dual 10D particle universe consists of two parallel particle-antiparticle universes with opposite energies and the bulk space separating the two universes. There are four space regions: the positive energy particle-antiparticle space region, the pregravity bulk space region, the negative energy particle-antiparticle space region, and the anti-pregravity bulk space region.

## 2.4.The Current Universe

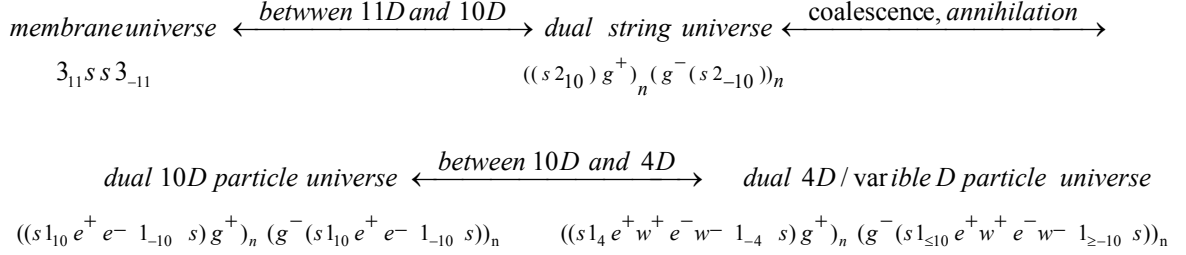
	Object structure	Space structure	Forces
The light universe	4D particle	attachment space and detachment space	strong, gravity, electromagnetic, and weak
The dark universe	variable D between 4 and 10 particle	attachment space	Pre-strong, gravity, pre-electromagnetic

The formation of our current universe follows immediately after the formation of the charged pre-universe through the asymmetrical dimensional oscillations, leading to the asymmetrical dual universe consisting of the light universe with kinetic energy and light and the dark universe without kinetic energy and light. Our observable universe is the light universe, whose formation involves the immediate transformation from 10D to 4D, resulting in the inflation as shown later. The formation of the dark universe involves the slow dimensional oscillation between 10D and 4D. The asymmetrical dual universe is manifested as the asymmetry in the weak interaction in our observable universe as follows.

$$((s1_4 e^+ w^+ e^- w^- 1_{-4} s)g^+)_n (g^-(s1_{\leq 10} e^+ w^+ e^- w^- 1_{\geq -10} s))_n \quad (16)$$

where s, g, e, and w are the strong force, gravity, electromagnetism, and weak interaction, respectively for the observable universe, and where  $1_{41-4}$  and  $1_{\leq 10} 1_{\geq -10}$  are 4D particle-antiparticle for the light universe and variable D particle-antiparticle for the dark universe, respectively.

In summary, the whole process of the local dimensional oscillations leading to our observable universe is illustrated as follows.



where s, e, and w are in the flat space, and g is in the bulk space. Each stage generates one force, so the four stages produce the four different forces: the strong force, gravity, electromagnetism, and the weak interaction, sequentially. Gravity appears in the first dimensional oscillation between the 11 dimensional membrane and the 10 dimensional string. The asymmetrical weak force appears in the asymmetrical second dimensional oscillation between the ten dimensional particle and the four dimensional particle. Charged electromagnetism appears as the force in the transition between the first and the second dimensional oscillations. The cosmology explains the origins of the four forces. To prevent the charged pre-universe to reverse back to the previous pre-universe, the charge pre-universe and the current universe overlap to a certain degree as shown in the overlapping between the electromagnetic interaction and the weak interaction to form the electroweak interaction.

The formation of the dark universe involves the slow dimensional oscillation between 10D and 4D. The dimensional oscillation for the formation of the dark universe involves the stepwise two-step transformation: the QVSL transformation and the varying supersymmetry transformation. In the normal supersymmetry transformation, the repeated application of the fermion-boson transformation carries over a boson (or fermion) from one point to the same boson (or fermion) at another point at the same mass. In the ‘‘varying supersymmetry transformation’’, the repeated application of the fermion-boson transformation carries over a boson from one point to the boson at another point at different mass dimension number in the same space-time number. The repeated varying supersymmetry transformation carries over a boson  $B_d$  into a fermion  $F_d$  and a fermion  $F_d$  to a boson  $B_{d-1}$ , which can be expressed as follows

$$M_{d,F} = M_{d,B} \alpha_{d,B}, \quad (17a)$$

$$M_{d-1,B} = M_{d,F} \alpha_{d,F}, \quad (17b)$$

where  $M_{d,B}$  and  $M_{d,F}$  are the masses for a boson and a fermion, respectively, d is the mass dimension number, and  $\alpha_{d,B}$  or  $\alpha_{d,F}$  is the fine structure constant that is the ratio between the masses of a boson and its fermionic partner. Assuming  $\alpha_{d,B}$  or  $\alpha_{d,F}$ , the relation

between the bosons in the adjacent dimensions or n dimensions apart (assuming  $\alpha$ 's are the same) then can be expressed as

$$M_{d,B} = M_{d+1,B} \alpha_{d+n}^2 \quad (17c)$$

$$M_{d,B} = M_{d+n,B} \alpha_{d+n}^{2n} \quad (17d)$$

Eq. (18) show that it is possible to describe mass dimensions  $> 4$  in the following way

$$F_5 B_5 F_6 B_6 F_7 B_7 F_8 B_8 F_9 B_9 F_{10} B_{10} F_{11} B_{11}, \quad (18)$$

where the energy of  $B_{11}$  is the Planck energy. Each mass dimension between 4d and 11d consists of a boson and a fermion. Eq. (19) show a stepwise transformation that converts a particle with d mass dimension to  $d \pm 1$  mass dimension.

$$D, d \xleftarrow{\text{stepwise varying supersymmetry}} D, (d \pm 1) \quad (19)$$

The transformation from a higher mass dimensional particle to the adjacent lower mass dimensional particle is the fractionalization of the higher dimensional particle to the many lower dimensional particle in such way that the number of lower dimensional particles becomes  $n_{d-1} = n_d / \alpha^2$ . The transformation from lower dimensional particles to higher dimensional particle is a condensation. Both the fractionalization and the condensation are stepwise. For example, a particle with 4D (space-time) 10d (mass dimension) can transform stepwise into 4D9d particles. Since the supersymmetry transformation involves translation, this stepwise varying supersymmetry transformation leads to a translational fractionalization and translational condensation, resulting in expansion and contraction.

For the formation of the dark universe from the charged pre-universe, the negative energy universe has the 10D4d particles, which is converted eventually into 4D4d stepwise and slowly. It involves the stepwise two-step varying transformation: first the QVSL transformation, and then, the varying supersymmetry transformation as follows.

stepwise two - step varying transform ation

$$(1) D, d \xleftarrow{\text{QVSL}} (D \mp 1), (d \pm 1) \quad (20)$$

$$(2) D, d \xleftarrow{\text{varying supersymmetry}} D, (d \pm 1)$$

The repetitive stepwise two-step transformations from 10D4d to 4D4d are as follows.

*The Hidden Dark Universe and the Observable Dark Universe with Dark Energy*

$$10D4d \rightarrow 9D5d \rightarrow 9D4d \rightarrow 8D5d \rightarrow 8D4d \rightarrow 7D5d \rightarrow \dots \rightarrow 5D4d \rightarrow 4D5d \rightarrow 4D4d$$

$\mapsto$  the hidden dark universe  $\leftrightarrow$  dark energy  $\leftarrow$

The dark universe consists of two periods: the hidden dark universe and the dark energy universe. The hidden dark universe composes of the  $> 4D$  particles. As mentioned before, particles with different space-time dimensions are transparent and oblivious to one another, and separate from one another if possible. Thus,  $> 4D$  particles are hidden and separated particles with respect to  $4D$  particles in the light universe (our observable universe). The universe with  $> 4D$  particles is the hidden dark universe. The  $4D$  particles transformed from hidden  $> 4D$  particles in the dark universe are observable dark energy for the light universe, resulting in the accelerated expanding universe. The accelerated expanding universe consists of the positive energy  $4D$  particles-antiparticles and dark energy that includes the negative energy  $4D$  particles-antiparticles and the antigravity. Since the dark universe does not have detachment space, the presence of dark energy is not different from the presence of the non-zero vacuum energy. In terms of quintessence, such dark energy can be considered the tracking quintessence [24] from the dark universe with the space-time dimension as the tracker. The tracking quintessence consists of the hidden quintessence and the observable quintessence. The hidden quintessence is from the hidden  $> 4D$  dark universe. The observable quintessence is from the observable  $4D$  dark universe with  $4D$  space-time.

For the formation of the light universe, the dimensional oscillation for the positive energy universe transforms  $10D$  to  $4D$  immediately. It involves the leaping two-step varying transformation, resulting in the light universe with kinetic energy. The first step is the space-time dimensional oscillation through QVSL. The second step is the mass dimensional oscillation through slicing-fusion.

*leaping two – step varying transformation*

$$(1) D, d \xleftarrow{\text{QVSL}} (D \mp n), (d \pm n) \quad (21)$$

$$(2) D, d \xleftarrow{\text{slicing - fusion}} D, (d \pm n) + (11 - d + n) \text{DO's}$$

The Light Universe

$$10D4d \xrightarrow{\text{quick QVSL transformation}} 4D10d \xrightarrow{\text{slicing with detachment space, inflation}} \\ \text{dark matter } (4D10d + 4D9d + 4D8d + 4D7d + 4D6d + 4D5d) + \text{baryonic matter } (4D4d) + \text{cosmic radiation} \\ \rightarrow \text{thermal cosmic expansion (the big bang)}$$

In the charged pre-universe, the positive energy universe has  $10D4d$ , which is transformed into  $4D10d$  in the first step through the QVSL transformation. The second step of the leaping varying transformation involves the slicing-fusion of particle. Bounias and Krasnoholovets [25] propose another explanation of the reduction of  $> 4D$  space-time into  $4D$  space-time by slicing  $> 4D$  space-time into infinitely many  $4D$  quantized units surrounding the  $4D$  core particle. Such slicing of  $> 4D$  space-time is like slicing  $3D$  space  $D$  object into  $2D$  space  $D$  object in the way stated by Michel Bounias as follows: “You cannot put a pot into a sheet without changing the shape of the  $2D$  sheet into a  $3D$  dimensional packet. Only a  $2D$  slice of the pot could be a part of sheet”.

The slicing is by detachment space, as a part of the space structure, which consists of attachment space (denoted as 1) and detachment space (denoted as 0) as described earlier. Attachment space attaches to object permanently with zero speed or reversibly at

the speed of light. Detachment space irreversibly detaches from the object at the speed of light. Attachment space relates to rest mass, while detachment space relates to kinetic energy. The cosmic origin of detachment space is the cosmic radiation from the particle-antiparticle annihilation that initiates the transformation. The cosmic radiation cannot permanently attach to a space.

The slicing of dimensions is the slicing of mass dimensions. 4D10d particle is sliced into seven particles: 4D10d, 4D9d, 4D8d, 4D7d, 4D6d, 4D5d, and 4D4d equally by mass. Baryonic matter is 4D4d, while dark matter consists of the other six types of particles (4D10d, 4D9d, 4D8d, 4D7d, 4D6d, and 4D5d) as described later. The mass ratio of dark matter to baryonic matter is 6 to 1 in agreement with the observation [26] showing the universe consists of 23% dark matter, 4% baryonic matter, and 73% dark energy.

Detachment space (0) involves in the slicing of mass dimensions. Attachment space is denoted as 1. For example, the slicing of 4D10d particles into 4D4d particles is as follows.

$$\begin{aligned} \left(1_{4+6}\right)_i & \xrightarrow{\text{slicing}} \left(1_4\right)_i + \sum_1^6 \left(\left(0_4\right)\left(1_4\right)\right)_{j,6} \\ & >4d \text{ attachment space} \quad 4d \text{ core attachment space} \quad 6 \text{ types of } 4d \text{ units} \end{aligned} \quad (22)$$

The two products of the slicing are the 4d-core attachment space and 6 types of 4d quantized units. The 4d core attachment space surrounded by 6 types of many (j) 4D4d quantized units corresponds to the core particle surrounded by 6 types of many small 4d particles.

Therefore, the transformation from d to d – n involves the slicing of a particle with d mass dimension into two parts: the core particle with d – n dimension and the n dimensions that are separable from the core particle. Such n dimensions are denoted as n “dimensional orbitals”, which become gauge force fields as described later. The sum of the number of mass dimensions for a particle and the number of dimensional orbitals (DO’s) is equal to 11 (including gravity) for all particles with mass dimensions. Therefore,

$$F_d = F_{d-n} + (11-d+n)\text{DO's} \quad (23)$$

where 11 – d + n is the number of dimensional orbitals (DO’s) for  $F_{d-n}$ . Thus, 4D10d particles can transformed into 4D10d, 4D9d, 4D8d, 4D7d, 4D6d, 4D5d, and 4D4d core particles, which have 1, 2, 3, 4, 5, 6, and 7 separable dimensional orbitals, respectively. Dark matter particle, 4D10d, has only gravity, while baryonic matter particle, 4D4d, has gravity and six other dimensional orbitals as gauge force fields as below.

The six > 4d mass dimensions (dimensional orbitals) for the gauge force fields and the one mass dimension for gravity are as in Figure 1.

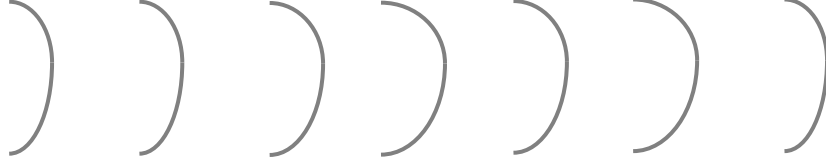


Figure 1. The seven force fields as  $> 4d$  mass dimensions (dimensional orbitals).

The dimensional orbitals of baryonic matter provide the base for the periodic table of elementary particles to calculate accurately the masses of all 4D elementary particles, including quarks, leptons, and gauge bosons as described later.

The lowest dimensional orbital is for electromagnetism. Baryonic matter is the only one with the lowest dimensional orbital for electromagnetism. With higher dimensional orbitals, dark matter does not have this lowest dimensional orbital. Without electromagnetism, dark matter cannot emit light, and is incompatible to baryonic matter, like the incompatibility between oil and water. The incompatibility between dark matter and baryonic matter leads to the inhomogeneity (like emulsion), resulting in the formation of galaxies, clusters, and superclusters as described later. Dark matter has not been found by direct detection because of the incompatibility.

In the light universe, the inflation is the leaping varying transformation that is the two-step inflation. The first step is to increase the rest mass as potential from higher space-time dimension to lower space-time dimension as expressed by Eq. (24a) from Eq. (11b).

$$\begin{aligned}
 D, d &\xrightarrow{QVSL} (D \mp n), (d \pm n) \\
 V_{D,d} &= V_{D-n, d+n} \alpha^{2n} \\
 \varphi &= \text{collective } n\text{'s} \\
 V(\varphi) &= V_{4D10d} \alpha^{-2\varphi}, \text{ where } \varphi \leq 0 \text{ from } -6 \text{ to } 0
 \end{aligned}
 \tag{24a}$$

where  $\alpha$  is the fine structure constant for electromagnetism. The ratio of the potential energies of 4D10d to that of 10D4d is  $1/\alpha^{12}$ .  $\varphi$  is the scalar field for QVSL, and is equal to collective  $n$ 's as the changes in space-time dimension number for many particles. The increase in the change of space-time dimensions from 4D decreases the potential as the rest mass. The region for QVSL is  $\varphi \leq 0$  from -6 to 0. The QVSL region is for the conversion of the vacuum energy into the rest mass as the potential. The conversion of vacuum energy into potential is equivalent to the absorption of the Higgs boson, while the conversion of potential into vacuum energy is equivalent to the emission of the Higgs boson.

The second step is the slicing that occurs simultaneously with the appearance of detachment space that is the space for cosmic radiation (photon). Potential energy as massive 4D10d particles is converted into kinetic energy as cosmic radiation and massive matter particles (from 10d to 4d). It relates to the ratio between photon and matter in terms of the CP asymmetry between particle and antiparticle. The slight excess particle over antiparticle results in matter particle. The equation for the potential (V) and the

scalar field ( $\phi$ ) is as Eq. (24b) from Eq. (35) that expresses the ratio between photon and matter.

$$D, d \xrightarrow{\text{slicing}} D, (d-n)$$

$$V(\phi) = V_{4D10d} \alpha^{2\phi}, \text{ where } \phi \geq 0 \text{ from } 0 \text{ to } 2$$
(24b)

The ratio is  $\alpha^4$ , according to Eq. (35). The region for the slicing is  $\phi \geq 0$  from 0 to 2. The slicing region is for the conversion of the potential energy into the kinetic energy.

The combination of Eq. (24a) and Eq. (24b) is as Eq. (24c).

$$V(\varphi, \phi) = V_{4D10d} (\alpha^{-2\varphi} + \alpha^{2\phi}),$$

$$\text{where } \varphi \leq 0 \text{ and } \phi \geq 0$$
(24c)

The graph for the two-step inflation is as Figure 2.

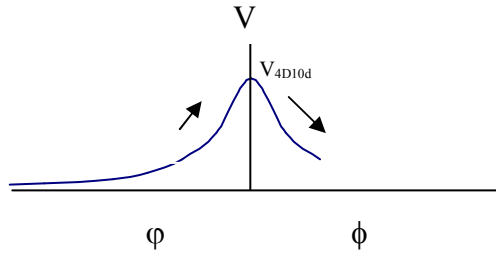


Figure 2. the two-step inflation

At the transition ( $V_{4D10d}$ ) between the first step (QVSL) and the second step (slicing), the scalar field reverses its sign and direction. In the first step, the universe inflates by the decrease in vacuum energy. In the second step, the potential energy is converted into kinetic energy as cosmic radiation. The resulting kinetic energy starts the big bang, resulting in the expanding universe.

Toward the end of the cosmic contraction after the big crunch, the deflation occurs as the opposite of the inflation. The kinetic energy from cosmic radiation decreases, as the fusion occurs to eliminate detachment space, resulting in the increase of potential energy. At the end of the fusion, the force fields except gravity disappear, 4D10d particles appear, and then the scalar field reverses its sign and direction. The vacuum energy increases as the potential as the rest mass decreases for the appearance of 10D4d particles, resulting in the end of a dimensional oscillation as Figure 3 for the two-step deflation.

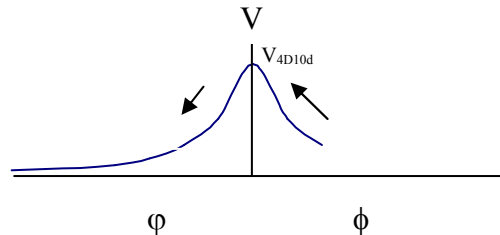


Figure 3. the two-step deflation

The end of the two-step deflation is 10D4d, which is followed immediately by the dimensional oscillation to return to 4D10d as the “dimensional bounce” as shown in Figure 4, which describes the dimensional oscillation from the left to the right: the beginning (inflation as 10D4d through 4D10d to 4D4d), the cosmic expansion-contraction, the end (deflation as 4D4d through 4D10d to 10D4d), the beginning (inflation), the cosmic expansion-contraction, and the end (deflation).

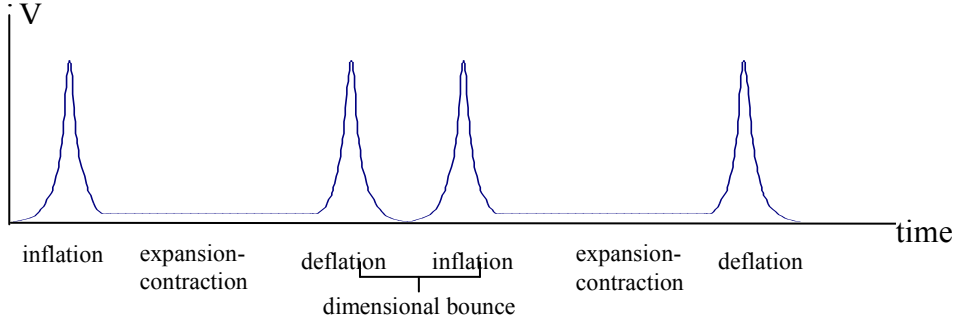


Figure 4. the cyclic observable universe by the dimensional oscillation

The two-step inflation corresponds to the quintom inflation. The symmetry breaking for the light universe can be described by quintom. Quintom [27] [28] [29] is the combination of quintessence and phantom. Quintessence describes a time-varying equation of state parameter,  $w$ , the ratio of its pressure to energy density and  $w > -1$ .

$$L_{quintessenc} = \frac{1}{2}(\partial_{\mu}\phi)^2 - V(\phi) \quad (25)$$

$$w = \frac{\dot{\phi}^2 - 2V(\phi)}{\dot{\phi}^2 + 2V(\phi)} \quad (26)$$

$$-1 \leq w \leq +1$$

Quintom includes phantom with  $w < -1$ . It has opposite sign of kinetic energy.

$$L_{phantom} = \frac{-1}{2}(\partial_{\mu}\phi)^2 - V(\phi) \quad (27)$$

$$w = \frac{-\dot{\phi}^2 - 2V(\phi)}{-\dot{\phi}^2 + 2V(\phi)} \quad (28)$$

$$-1 \geq w$$

As the combination of quintessence and phantom from Eqs. (24), (25), (26), and (27), quintom is as follows.

$$L_{quintessenc} = \frac{1}{2}(\partial_{\mu}\phi)^2 - \frac{1}{2}(\partial_{\mu}\varphi)^2 - V(\phi) - V(\varphi) \quad (29)$$

$$w = \frac{\dot{\phi}^2 - \dot{\varphi}^2 - 2V(\phi) - 2V(\varphi)}{\dot{\phi}^2 - \dot{\varphi}^2 + 2V(\phi) + 2V(\varphi)} \quad (30)$$

Phantom represents the scalar field  $\varphi$  in the space-time dimensional oscillation in QVSL, while quintessence represents the scalar field  $\phi$  in the mass dimensional oscillation in the slicing-fusion. Since QVSL does not involve kinetic energy, the physical source of the negative kinetic energy for phantom is the increase in vacuum energy or the emission of the Higgs boson, resulting in the decrease in energy density and pressure with respect to the observable potential,  $V(\varphi)$ . Combining Eqs. (24c) and (30), quintom is as follows.

$$\begin{aligned} w &= \frac{\dot{\phi}^2 - \dot{\varphi}^2 - 2V(\phi) - 2V(\varphi)}{\dot{\phi}^2 - \dot{\varphi}^2 + 2V(\phi) + 2V(\varphi)} \\ &= \frac{\dot{\phi}^2 - \dot{\varphi}^2 - 2V_{4D10d}(\alpha^{-2\varphi} + \alpha^{2\phi})}{\dot{\phi}^2 - \dot{\varphi}^2 + 2V_{4D10d}(\alpha^{-2\varphi} + \alpha^{2\phi})} \end{aligned} \quad (31)$$

where  $\varphi \leq 0$  and  $\phi \geq 0$

Figure 5 shows the plot of the evolution of the equation of state  $w$  for the quintom inflation.

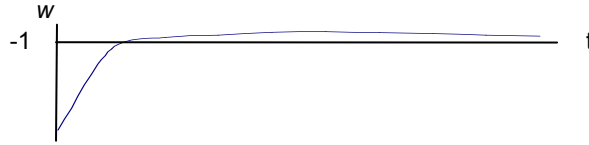


Figure 5. the  $w$  of quintom for the quintom inflation

Figure 6 shows the plot of the evolution of the equation of state  $w$  for the cyclic universe as Figure 4.

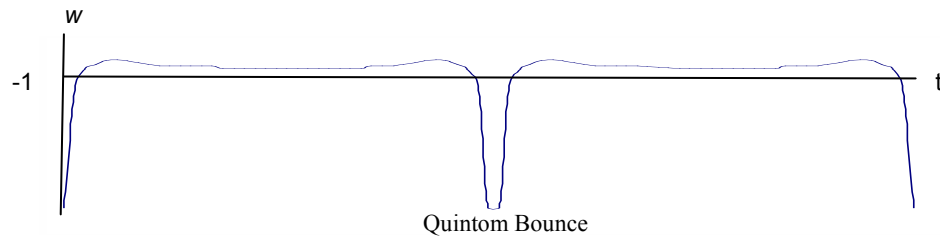


Figure 6. the cyclic universe by the dimensional oscillation as Figure 4

In the dimensional bounce in the middle of Figure 6, the equation of state crosses  $w = -1$  twice as also shown in the recent development of the quintom model [30] [31] in which, for the Quintom Bounce, the equation of state crosses the cosmological constant boundary twice around the bounce point to start another cycle of the dual universe.

The hidden dark universe with  $D > 4$  and the observable universe with  $D = 4$  are the “parallel universes” separated from each other by the bulk space. When the slow QVSL transformation of 5D hidden particles in the hidden universe into observable 4D particles, the observable 4 D particles become the dark energy for the observable universe. At a certain time, the hidden universe disappears, and becomes completely observable as dark energy. The maximum connection of the two universes includes the positive energy particle-antiparticle space region, the gravity bulk space region, the negative energy particle-antiparticle space region, and the anti-gravity bulk space region. Through the symmetry among the space regions, all regions expand synchronically and equally. (The symmetry is necessary for the ultimate reversibility of all cosmic processes.) The minimum observable universe has only one of the four space regions before the emergence of dark energy, when the light universe and the dark universe are separated from each other by the bulk space. The present observable universe about reaches the maximum at the observed 73% dark energy [26], about equal to the three additional space regions to the one original space region.

After the maximally connected universe, 4D dark energy transforms back to  $> 4D$  particles that are not observable. The removal of dark energy in the observable universe results in the stop of accelerated expansion and the start of contraction of the observable universe.

The end of dark energy starts another “parallel universe period”. Both hidden universe and observable universe contract synchronically and equally. Eventually, gravity causes the observable universe to crush to lose all cosmic radiation, resulting in the return to 4D10d particles under the deflation. The increase in vacuum energy allows 4D10d particles to become positive energy 10D4d particles-antiparticle. Meanwhile, hidden  $> 4D$  particles-antiparticles in the hidden universe transform into negative energy 10D4d particles-antiparticles. The dual universe can undergo another cycle of the dual universe with the dark and light universes. On the other hand, both universes can undergo transformation by the reverse isodual hole theory to become dual 10D string universe, which in turn can return to the 11D membrane universe as the multiverse background as follows.

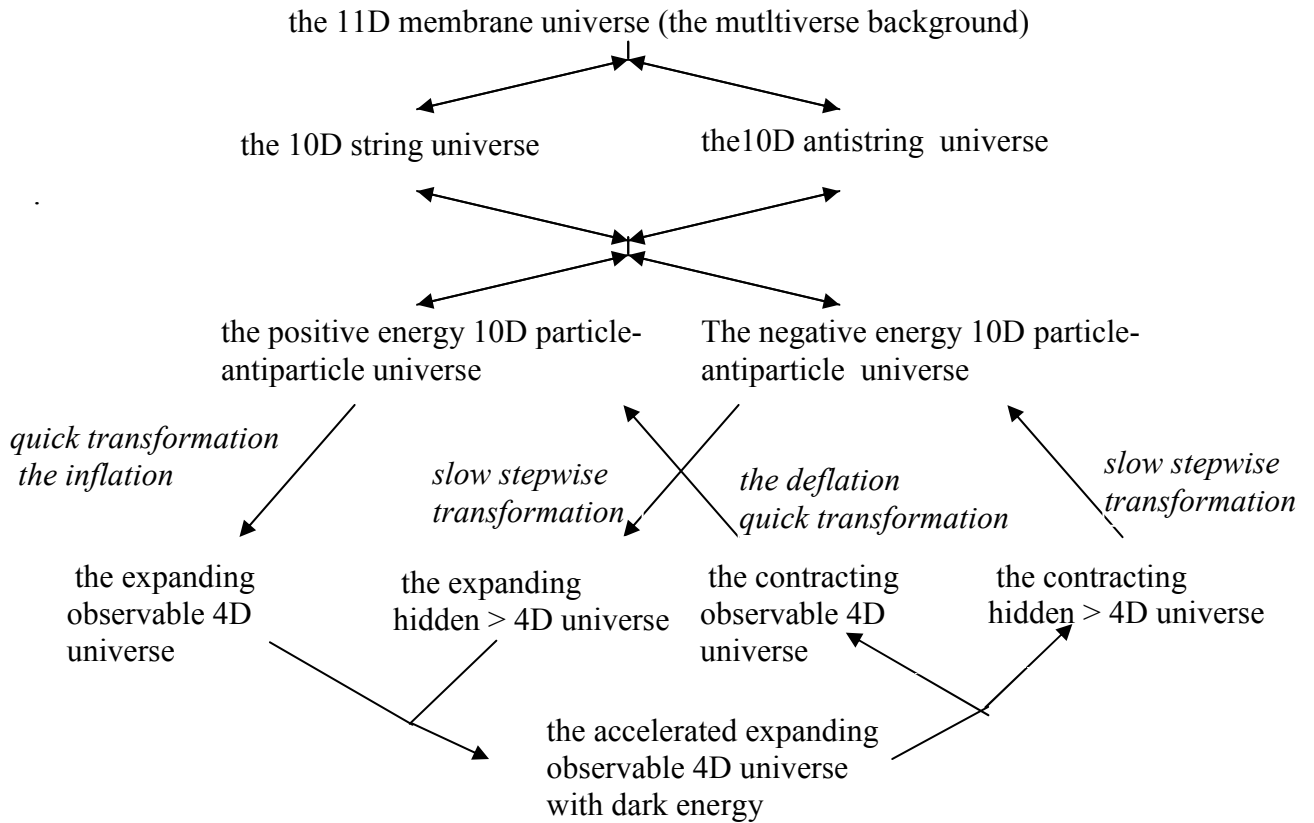


**Figure 7.** Cosmology

## 2.5. The Periodic Table of Elementary Particles

### 2.5.1. The CP Asymmetry

In the light universe, cosmic radiation is the result of the annihilation of the CP symmetrical particle-antiparticle. However, there is the CP asymmetry, resulting in excess of matter. Matter results from the combination of the CP asymmetrical particle-antiparticle. A baryonic matter particle (4d) has seven dimensional orbitals. The CP asymmetrical particle-antiparticle particle means the combination of two asymmetrical sets of seven from particle and antiparticle, resulting in the combination of the seven “principal dimensional orbitals” and the seven “auxiliary dimensional orbitals”. The auxiliary orbitals are dependent on the principal orbitals, so a baryonic matter particle appears to have only one set of dimensional orbitals. For baryonic matter, the principal dimensional orbitals are for leptons and gauge bosons, and the auxiliary dimensional orbitals are mainly for individual quarks. Because of the dependence of the auxiliary dimensional orbitals, individual quarks are hidden. In other words, there is asymmetry between lepton and quark, resulting in the survival of matter without annihilation. The configuration of dimensional orbitals and the periodical table of elementary particles [32] are shown in Fig. 8 and Table 1.

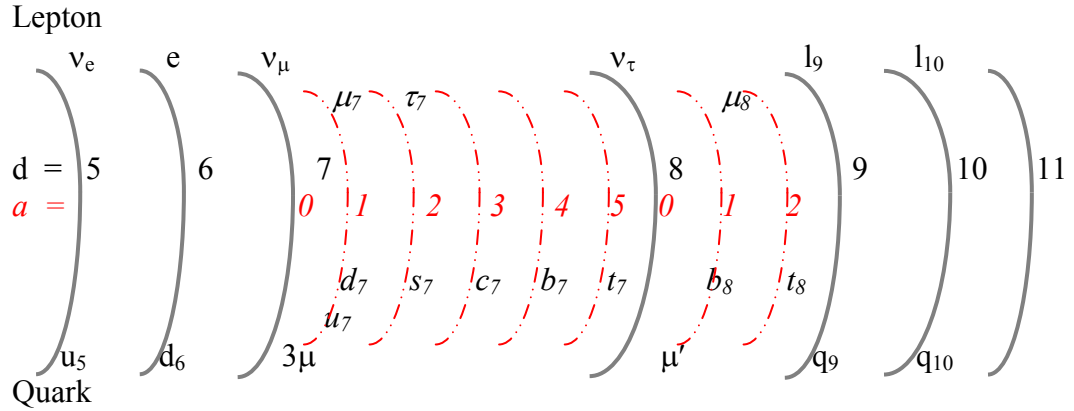


**Fig. 8:** leptons and quarks in the principal and auxiliary dimensional orbitals  $d =$  principal dimensional orbital (solid line) number,  $a =$  auxiliary dimensional orbital (dot line) number

**Table 1.** The Periodic Table of Elementary Particles

$d =$  principal dimensional orbital number,  $a =$  auxiliary dimensional orbital number

D	a=0	1	2	a=0	1	2	3	4	5	
	<u>Lepton</u>			<u>Quark</u>						<u>Boson</u>
5	$l_5 = v_e$			$q_5 = u = 3v_e$					$B_5 = A$	
6	$l_6 = e$			$q_6 = d = 3e$					$B_6 = \pi_{1/2}$	
7	$l_7 = v_\mu$	$\mu_7$	$\tau_7$	$q_7 = 3\mu$	$u_7/d_7$	$s_7$	$c_7$	$b_7$	$t_7$	$B_7 = Z_L^0$
8	$l_8 = v_\tau$	$\mu_8$ (empty)		$q_8 = \mu'$	$b_8$	$t_8$ (empty)				$B_8 = X_R$
9	$l_9$			$q_9$						$B_9 = X_L$
10										$B_{10} = Z_R^0$
11										$B_{11}$

In Fig. 8 and Table 1,  $d$  is the principal dimensional orbital number, and  $a$  is the auxiliary dimensional orbital number. (Note that  $F_d$  has lower energy than  $B_d$ .)

### 2.5.2. The Boson Mass Formula

The principal dimensional orbitals are for gauge bosons of the force fields. For the gauge bosons, the seven orbitals of principal dimensional orbital are arranged as  $F_5 B_5 F_6 B_6 F_7 B_7 F_8 B_8 F_9 B_9 F_{10} B_{10} F_{11} B_{11}$ , where  $B$  and  $F$  are boson and fermion in each orbital. The mass dimension in Eq. (17) becomes the orbitals in dimensional orbital with the same equations.

$$M_{d,F} = M_{d,B} \alpha_{d,B}, \quad (32a)$$

$$M_{d-1,B} = M_{d,F} \alpha_{d,F}, \quad (32b)$$

$$M_{d-1,B} = M_{d,B} \alpha_d^2. \quad (32c)$$

where D is the dimensional orbital number from 6 to 11.  $E_{5,B}$  and  $E_{11,B}$  are the energies for the 5d dimensional orbital and the 11d dimensional orbital, respectively. The lowest energy is the Coulombic field,

$$E_{5,B} = \alpha E_{6,F} = \alpha M_e. \quad (33)$$

The bosons generated are the dimensional orbital bosons or  $B_D$ . Using only  $\alpha_e$ , the mass of electron ( $M_e$ ), the mass of  $Z^0$ , and the number (seven) of dimensional orbitals, the masses of  $B_D$  as the gauge boson can be calculated as shown in Table 2.

**Table 2.** The Masses of the dimensional orbital bosons:

$\alpha = \alpha_e$ , d = dimensional orbital number

$B_d$	$M_d$	GeV (calculated)	Gauge boson	Interaction, symmetry	Predecessor
$B_5$	$M_e \alpha$	$3.7 \times 10^{-6}$	A	Electromagnetic, U(1)	Pre-charged
$B_6$	$M_e/\alpha$	$7 \times 10^{-2}$	$\pi_{1/2}$	Strong, SU(3)	Pre-strong
$B_7$	$M_6/\alpha_w^2 \cos \theta_w$	91.177 (given)	$Z_L^0$	weak (left), SU(2) <sub>L</sub>	Fractionalization (slicing)
$B_8$	$M_7/\alpha^2$	$1.7 \times 10^6$	$X_R$	CP (right) nonconservation	CP asymmetry
$B_9$	$M_8/\alpha^2$	$3.2 \times 10^{10}$	$X_L$	CP (left) nonconservation	CP asymmetry
$B_{10}$	$M_9/\alpha^2$	$6.0 \times 10^{14}$	$Z_R^0$	weak (right)	Fractionalization (slicing)
$B_{11}$	$M_{10}/\alpha^2$	$1.1 \times 10^{19}$	G	Gravity	Pregravity

In Table 2,  $\alpha = \alpha_e$  (the fine structure constant for electromagnetic field), and  $\alpha_w = \alpha/\sin^2 \theta_w$ .  $\alpha_w$  is not same as  $\alpha$  of the rest, because as shown later, there is a mixing between  $B_5$  and  $B_7$  as the symmetry mixing between U(1) and SU(2) in the standard theory of the electroweak interaction, and  $\sin \theta_w$  is not equal to 1. (The symmetrical charged dual pre-universe overlaps with the current asymmetrical universe for the weak interaction as shown earlier.) As shown later,  $B_5$ ,  $B_6$ ,  $B_7$ ,  $B_8$ ,  $B_9$ , and  $B_{10}$  are A (massless photon),  $\pi_{1/2}$  (half of pion),  $Z_L^0$ ,  $X_R$ ,  $X_L$ , and  $Z_R^0$ , respectively, responsible for the electromagnetic field, the strong interaction, the weak (left handed) interaction, the CP (right handed) nonconservation, the CP (left handed) nonconservation, and the P (right handed) nonconservation, respectively. The calculated value for  $\alpha_w$  is 0.2973, and  $\theta_w$  is  $29.69^\circ$  in good agreement with  $29.31^\circ$  for the observed value of  $\theta_w$  [33]. The calculated energy for  $B_{11}$  is  $1.1 \times 10^{19}$  GeV in good agreement with the Planck mass,  $1.2 \times 10^{19}$  GeV. The strong interaction, representing by  $\pi_{1/2}$  (half of pion), is for the interactions among quarks, and for the hiding of individual quarks in the auxiliary orbital. The weak interaction, representing by  $Z_L^0$ , is for the interaction involving changing flavors (decomposition and condensation) among quarks and leptons.

There are dualities between dimensional orbitals and the cosmic evolution process. The pre-charged force, the pre-strong force, the fractionalization, the CP asymmetry, and the pregravity are the predecessors of electromagnetic force, the strong force, the weak

interaction, the CP nonconservation, and gravity, respectively. These forces are manifested in the dimensional orbitals with various space-time symmetries and gauge symmetries. The strengths of these forces are different than their predecessors, and are arranged according to the dimensional orbitals. Only the 4d particle (baryonic matter) has the  $B_5$ , so without  $B_5$ , dark matter consists of permanently neutral higher dimensional particles. It cannot emit light, cannot form atoms, and exists as neutral gas.

The principal dimensional boson,  $B_8$ , is a CP violating boson, because  $B_8$  is assumed to have the CP-violating  $U(1)_R$  symmetry. The ratio of the force constants between the CP-invariant  $W_L$  in  $B_8$  and the CP-violating  $X_R$  in  $B_8$  is

$$\begin{aligned} \frac{G_8}{G_7} &= \frac{\alpha E_7^2 \cos^2 \Theta_W}{\alpha_W E_8^2} \\ &= 5.3 \times 10^{-10} \quad , \end{aligned} \quad (34)$$

which is in the same order as the ratio of the force constants between the CP-invariant weak interaction and the CP-violating interaction with  $|\Delta S| = 2$ .

The principal dimensional boson,  $B_9$  ( $X_L$ ), has the CP-violating  $U(1)_L$  symmetry.  $B_9$  generates matter. The ratio of force constants between  $X_R$  with CP conservation and  $X_L$  with CP-nonconservation is

$$\begin{aligned} \frac{G_9}{G_8} &= \frac{\alpha E_8^2}{\alpha E_9^2} \\ &= \alpha^4 \\ &= 2.8 \times 10^{-9} \quad , \end{aligned} \quad (35)$$

which is the ratio of the numbers between matter (dark and baryonic) and photons in the universe. It is close to the ratio of the numbers between baryonic matter and photons about  $5 \times 10^{-10}$  obtained by the big bang nucleosynthesis.

Auxiliary dimensional orbital is derived from principal dimensional orbital. It is for high-mass leptons and individual quarks. Auxiliary dimensional orbital is the second set of the three sets of seven orbitals. The combination of dimensional auxiliary dimensional orbitals constitutes the periodic table for elementary particles as shown in Fig. 8 and Table 1.

There are two types of fermions in the periodic table of elementary particles: low-mass leptons and high-mass leptons and quarks. Low-mass leptons include  $\nu_e$ ,  $e$ ,  $\nu_\mu$ , and  $\nu_\tau$ , which are in principal dimensional orbital, not in auxiliary dimensional orbital.  $l_d$  is denoted as lepton with principal dimension number,  $d$ .  $l_5$ ,  $l_6$ ,  $l_7$ , and  $l_8$  are  $\nu_e$ ,  $e$ ,  $\nu_\mu$ , and  $\nu_\tau$ , respectively. All neutrinos have zero mass because of chiral symmetry (permanent chiral symmetry).

### 2.5.3. The Mass Composites of Leptons and Quarks

High-mass leptons and quarks include  $\mu$ ,  $\tau$ ,  $u$ ,  $d$ ,  $s$ ,  $c$ ,  $b$ , and  $t$ , which are the combinations of both principal dimensional fermions and auxiliary dimensional fermions. Each fermion can be defined by principal dimensional orbital numbers ( $d$ 's) and auxiliary dimensional orbital numbers ( $a$ 's) as  $d_a$  in Table 3. For examples,  $e$  is  $6_0$  that means it has  $d$

(principal dimensional orbital number) = 6 and a (auxiliary dimensional orbital number) = 0, so e is a principal dimensional fermion.

High-mass leptons,  $\mu$  and  $\tau$ , are the combinations of principal dimensional fermions, e and  $\nu_\mu$ , and auxiliary dimensional fermions. For example,  $\mu$  is the combination of e,  $\nu_\mu$ , and  $\mu_7$ , which is  $7_1$  that has  $d = 7$  and  $a = 1$ .

Quarks are the combination of principal dimensional quarks ( $q_d$ ) and auxiliary dimensional quarks. The principal dimensional fermion for quark is derived from principal dimensional lepton. To generate a principal dimensional quark in principal dimensional orbital from a lepton in the same principal dimensional orbital is to add the lepton to the boson from the combined lepton-antilepton. Thus, the mass of the quark is three times of the mass of the corresponding lepton in the same dimension. The equation for the mass of principal dimensional fermion for quark is

$$M_{q_d} = 3M_{l_d} \quad (36)$$

For principal dimensional quarks,  $q_5$  ( $5_0$ ) and  $q_6$  ( $6_0$ ) are  $3\nu_e$  and  $3e$ , respectively. Since  $l_7$  is massless  $\nu_\mu$ ,  $\nu_\mu$  is replaced by  $\mu$ , and  $q_7$  is  $3\mu$ . Quarks are the combinations of principal dimensional quarks,  $q_d$ , and auxiliary dimensional quarks. For example, s quark is the combination of  $q_6$  ( $3e$ ),  $q_7$  ( $3\mu$ ) and  $s_7$  (auxiliary dimensional quark =  $7_2$ ).

Each fermion can be defined by principal dimensional orbital numbers (d's) and auxiliary dimensional orbital numbers (a's). All leptons and quarks with d's, a's and the calculated masses are listed in Table 3.

**Table 3.** The Compositions and the Constituent Masses of Leptons and Quarks  
d = principal dimensional orbital number and a = auxiliary dimensional orbital number

	$d_a$	Composition	Calculated Mass
<u>Leptons</u>	<u><math>d_a</math> for leptons</u>		
$\nu_e$	$5_0$	$\nu_e$	0
e	$6_0$	e	0.51 MeV (given)
$\nu_\mu$	$7_0$	$\nu_\mu$	0
$\nu_\tau$	$8_0$	$\nu_\tau$	0
$\mu$	$6_0 + 7_0 + 7_1$	$e + \nu_\mu + \mu_7$	105.6 MeV
$\tau$	$6_0 + 7_0 + 7_2$	$e + \nu_\mu + \tau_7$	1786 MeV
$\mu'$	$6_0 + 7_0 + 7_2 + 8_0 + 8_1$	$e + \nu_\mu + \mu_7 + \nu_\tau + \mu_8$	136.9 GeV
<u>Quarks</u>	<u><math>d_a</math> for quarks</u>		
u	$5_0 + 7_0 + 7_1$	$q_5 + q_7 + u_7$	330.8 MeV
d	$6_0 + 7_0 + 7_1$	$q_6 + q_7 + d_7$	332.3 MeV
s	$6_0 + 7_0 + 7_2$	$q_6 + q_7 + s_7$	558 MeV
c	$5_0 + 7_0 + 7_3$	$q_5 + q_7 + c_7$	1701 MeV
b	$6_0 + 7_0 + 7_4$	$q_6 + q_7 + b_7$	5318 MeV
t	$5_0 + 7_0 + 7_5 + 8_0 + 8_2$	$q_5 + q_7 + t_7 + q_8 + t_8$	176.5 GeV

### 2.5.4. The Lepton Formula

The principal dimensional fermion for heavy leptons ( $\mu$  and  $\tau$ ) is  $e$  and  $\nu_e$ . Auxiliary dimensional fermion is derived from principal dimensional boson in the same way as Eq. (32) to relate the energies for fermion and boson. For the mass of auxiliary dimensional fermion (AF) from principal dimensional boson (B), the equation is Eq. (37).

$$M_{AF_{d,a}} = \frac{M_{B_{d-1,0}}}{\alpha_a} \sum_{a=0}^a a^4, \quad (37)$$

where  $\alpha_a$  = auxiliary dimensional fine structure constant, and  $a$  = auxiliary dimension number = 0 or integer. The first term,  $\frac{M_{B_{d-1,0}}}{\alpha_a}$ , of the mass formula (Eq.(37)) for the auxiliary dimensional fermions is derived from the mass equation, Eq. (32), for the principal dimensional fermions and bosons. The second term,  $\sum_{a=0}^a a^4$ , of the mass formula is for Bohr-Sommerfeld quantization for a charge - dipole interaction in a circular orbit as described by A. Barut [34]. As in Barut lepton mass formula,  $1/\alpha_a$  is  $3/2$ . The coefficient,  $3/2$ , is to convert the principal dimensional boson mass to the mass of the auxiliary dimensional fermion in the higher dimension by adding the boson mass to its fermion mass which is one-half of the boson mass. Using Eq. (32), Eq. (37) becomes the formula for the mass of auxiliary dimensional fermions (AF).

$$\begin{aligned} M_{AF_{d,a}} &= \frac{3M_{B_{d-1,0}}}{2} \sum_{a=0}^a a^4 \\ &= \frac{3M_{F_{d-1,0}}}{2\alpha_{d-1}} \sum_{a=0}^a a^4 \\ &= \frac{3}{2} M_{F_{d,0}} \alpha_d \sum_{a=0}^a a^4 \end{aligned} \quad (38)$$

The mass of this auxiliary dimensional fermion is added to the sum of masses from the corresponding principal dimensional fermions (F's) with the same electric charge or the same dimension. The corresponding principal dimensional leptons for  $u$  ( $2/3$  charge) and  $d$  ( $-1/3$  charge) are  $\nu_e$  (0 charge) and  $e$  ( $-1$  charge), respectively, by adding  $-2/3$  charge to the charges of  $u$  and  $d$  [35]. The fermion mass formula for heavy leptons is derived as follows.

$$\begin{aligned} M_{F_{d,a}} &= \sum M_F + M_{AF_{d,a}} \\ &= \sum M_F + \frac{3M_{B_{d-1,0}}}{2} \sum_{a=0}^a a^4 \end{aligned} \quad (39a)$$

$$= \sum M_F + \frac{3M_{F_{d-1,0}}}{2\alpha_{d-1}} \sum_{a=0}^a a^4 \quad (39b)$$

$$= \sum M_F + \frac{3}{2} M_{F_{d,0}} \alpha_d \sum_{a=0}^a a^4 \quad (39c)$$

Eq. (39b) is for the calculations of the masses of leptons. The principal dimensional fermion in the first term is e. Eq. (39b) can be rewritten as Eq. (40).

$$M_a = M_e + \frac{3M_e}{2\alpha} \sum_{a=0}^a a^4, \quad (40)$$

a = 0, 1, and 2 are for e,  $\mu$ , and  $\tau$ , respectively. It is identical to the Barut lepton mass formula.

### 2.5.5. The Quark Mass Formula

The auxiliary dimensional quarks except a part of t quark are  $q_7$ 's. Eq.(39c) is used to calculate the masses of quarks. The principal dimensional quarks include  $3\nu_\mu$ ,  $3e$ , and  $3\mu$ ,  $\alpha_7 = \alpha_w$ , and  $q_7 = 3\mu$ . Eq. (39c) can be rewritten as the quark mass formula.

$$M_q = \sum M_F + \frac{3\alpha_w M_{3\mu}}{2} \sum_{a=0}^a a^4, \quad (41)$$

where a = 1, 2, 3, 4, and 5 for u/d, s, c, b, and a part of t, respectively.

To match  $l_8$  ( $\nu_\tau$ ), quarks include  $q_8$  as a part of t quark. In the same way that  $q_7 = 3\mu$ ,  $q_8$  involves  $\mu'$ .  $\mu'$  is the sum of e,  $\mu$ , and  $\mu_8$  (auxiliary dimensional lepton). Using Eq. (39a), the mass of  $\mu_8$  is equal to 3/2 of the mass of  $B_7$ , which is  $Z^0$ . Because there are only three families for leptons,  $\mu'$  is the extra lepton, which is "hidden".  $\mu'$  can appear only as  $\mu +$  photon. The pairing of  $\mu + \mu$  from the hidden  $\mu'$  and regular  $\mu$  may account for the occurrence of same sign dilepton in the high energy level [36]. The principal dimensional quark  $q_8 = \mu'$  instead of  $3\mu'$ , because  $\mu'$  is hidden, and  $q_8$  does not need to be  $3\mu'$  to be different. Using the equation similar to Eq.(41), the calculation for t quark involves  $\alpha_8 = \alpha$ ,  $\mu'$  instead of  $3\mu$  for principal fermion, and a = 1 and 2 for  $b_8$  and  $t_8$ , respectively. The hiding of  $\mu'$  for leptons is balanced by the hiding of  $b_8$  for quarks.

The calculated masses are in good agreement with the observed constituent masses of leptons and quarks [37]. The mass of the top quark [38] is  $174.3 \pm 5.1$  GeV in a good agreement with the calculated value, 176.5 GeV.

With the masses of quarks calculated by the periodic table of elementary particles, the masses of all hadrons can be calculated [32] as the composes of quarks, as molecules are the composes of atoms. The calculated values are in good agreement with the observed values. For examples, the calculated masses of neutron and pion are

939.54MeV, and 135.01MeV in excellent agreement with the observed masses, 939.57 MeV and 134.98 MeV, respectively. At different temperatures, the strong force (QCD) among quarks in hadrons behaves differently to follow different dimensional orbitals [33].

## 2.6. Summary

There are three stages of pre-universes in chronological order: the strong pre-universe, the gravitational pre-universe, and the charged pre-universe. The multiverse background is the strong pre-universe with the simplest expression of the cosmic code. Its object structure is 11D membrane and its space structure is attachment space only. The only force is the pre-strong force without gravity. The transformation from 11D membrane to 10D string results in the gravitational pre-universe with both pre-strong force and pre-gravity. The repulsive pre-gravity and pre-antigravity brings about the dual 10D string universe. The coalescence and the separation of the dual universe result in the dual charged universe as dual 10D particle universe with the pre-strong, pre-gravity, and pre-electromagnetic force fields.

The asymmetrical dimensional oscillations result in the asymmetrical dual universe: the light universe with light and kinetic energy and the dark universe without light and kinetic energy. The asymmetrical dimensional oscillation is manifested as the asymmetrical weak force field. The light universe is our observable universe. The dark universe is sometimes hidden, and is sometimes observable as dark energy. The dimensional oscillation for the dark universe is the slow dimensional oscillation from 10D and 4D. The dimensional oscillation for the light universe involves the immediate transformation from 10D to 4D and the introduction of detachment space, resulting in light and kinetic energy. For baryonic matter, the incorporation of detachment space for baryonic matter brings about “the dimensional orbitals” as the base for the periodic table of elementary particles for all leptons, quarks, and gauge bosons. The masses of gauge bosons, leptons, quarks can be calculated using only four known constants: the number of the extra spatial dimensions in the eleven-dimensional membrane, the mass of electron, the mass of  $Z^0$ , and the fine structure constant. The calculated values are in good agreement with the observed values. The differences in dimensional orbitals result in incompatible dark matter and baryonic matter.

## 3. The Galaxy Formation

### Introduction

The current observable universe contains dark energy, dark matter, and baryonic matter. As mentioned in the previous section, dark energy is from the dark universe to accelerate the expansion of the observable universe. Dark matter have different mass dimension from the baryonic matter. We live in the world of baryonic matter. The separation of baryonic matter and dark matter results in the galaxy formation.

#### 3.1. The Separation of Baryonic Matter and Dark Matter

Dark matter has been detected only indirectly by means of its gravitational effects astronomically. Dark matter as weakly interacting massive particles (WIMPs) has not been detected directly on the earth [39]. The previous section proposes that the absence of the direct detection of dark matter on the earth is due to the incompatibility between baryonic matter and dark matter, analogous to incompatible water and oil. The previous papers provide the reasons for the incompatibility and the mass ratio (6 to 1) of dark matter to baryonic matter. Basically, during the inflation before the big bang, dark matter, baryonic matter, cosmic radiation, and the gauge force fields are generated. There are six types of dark matter with the “mass dimensions” from 5 to 10, while baryonic matter has the mass dimension of 4. As a result, the mass ratio is 6 to 1 as observed. Without electromagnetism, dark matter cannot emit light, and is incompatible to baryonic matter. Like oil, dark matter is completely non-polar. The common link between baryonic matter and dark matter is the cosmic radiation resulted from the annihilation of matter and antimatter from both baryonic matter and dark matter. With the high concentration of cosmic radiation at the beginning of the big bang, baryonic matter and dark matter are completely compatible. As the universe ages and expands, the concentration of cosmic concentration decreases, resulting in the increasing incompatibility between baryonic matter and dark matter until the incompatibility reaches to the maximum value with low concentration of cosmic radiation.

The incompatibility is expressed in the form of the repulsive MOND (modified Newtonian dynamics) force field. MOND [40] proposes the deviation from the Newtonian dynamics in the low acceleration region in the outer region of a galaxy. This paper proposes the MOND forces in the interface between the baryonic matter region and the dark matter region [41]. In the interface, the same matter materials attract as the conventional attractive MOND force, and the different matter materials repulse as the repulsive MOND force between baryonic matter and dark matter.

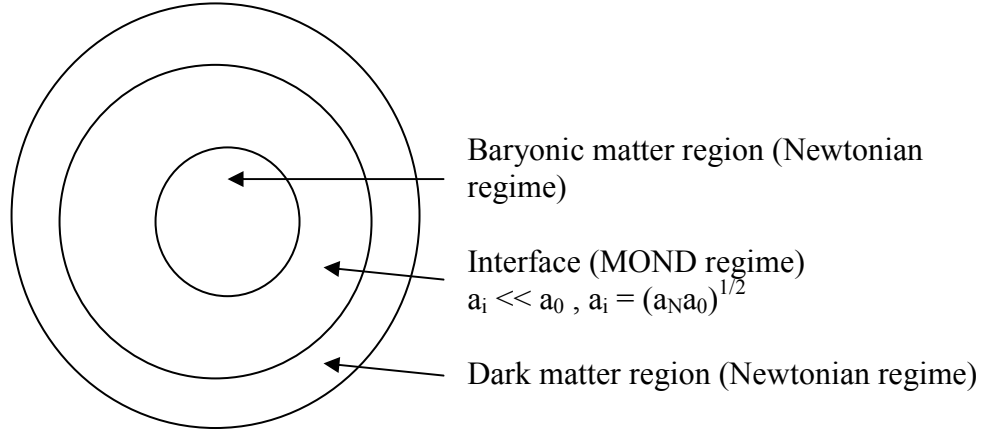


Figure 9: the interfacial region between the baryonic and the dark matter regions

In Figure 9, the inner part is the baryonic matter region, the middle part is the interface, and the outer part is the dark matter region. The MOND forces in the interface are the interfacial attractive force (conventional MOND force),  $F_{i-A}$ , among the same matter materials and the interfacial repulsive force (repulsive MOND force),  $F_{i-R}$ , between baryonic matter material and dark matter material. The interfacial repulsive force enhances the interfacial attractive force toward the center of gravity in terms of the interfacial acceleration,  $a_i$ .

The border between the baryonic matter region and the interface is defined by the acceleration constant,  $a_0$ . The interfacial acceleration is less than  $a_0$ . The enhancement is expressed as the square root of the product of  $a_i$  and  $a_0$ . In the baryonic matter region,  $a_b$  is greater than  $a_0$ , and is equal to normal Newtonian acceleration as Eq. (42).

$$\begin{aligned}
 a_0 &<< a_b, & a_b &= a_N \text{ in the baryonic matter region} \\
 a_0 &>> a_i, & a_i &= \sqrt{a_N a_0} \text{ in the interfacial region}
 \end{aligned}
 \tag{42}$$

The interfacial attractive force in the interface with the baryonic matter region is expressed as Eq. (43) where  $m$  is the mass of baryonic material in the interface.

$$\begin{aligned}
 F_{i-A} &= ma_N \\
 &= m \frac{a_i^2}{a_0},
 \end{aligned}
 \tag{43}$$

The comparison of the interfacial attractive force,  $F_{i-A}$ , and the non-existing interfacial Newtonian attractive force,  $F_{i-Newton}$  in the interface is as Eqs. (44), (45), and (46), where  $G$  is the gravitation constant,  $M$  is the mass of the baryonic material, and  $r$  the distance between the gravitational center and the material in the infacial region.

$$\begin{aligned}
F_{i-A} &= \frac{GMm}{r^2} \\
&= m \frac{a^2}{a_0},
\end{aligned} \tag{44}$$

$$\begin{aligned}
F_{i-Newton} &= \frac{GMm}{r^2} \\
&= m a
\end{aligned}$$

$$a_i = \frac{\sqrt{GMa_0}}{r} \tag{45}$$

$$a_{i-Newton} = \frac{GM}{r^2},$$

$$F_{i-A} = \frac{m\sqrt{GMa_0}}{r} \tag{46}$$

$$F_{i-Newton} = \frac{mGM}{r^2},$$

The interfacial attractive force decays with  $r$ , while the interfacial Newtonian force decays with  $r^2$ . Therefore, in the interface when  $a_0 \gg a_i$ , with sufficient dark matter, the interfacial repulsive force,  $F_{i-R}$ , is the difference between the interfacial attractive force and the interfacial Newtonian force as Eq. (47).

$a_0 \gg a_i$ , in the interfacial region

$$\begin{aligned}
F_{i-R} &= F_{i-A} - F_{i-Newton} \\
&= m \left( \frac{\sqrt{GMa_0}}{r} - \frac{GM}{r^2} \right)
\end{aligned} \tag{47}$$

The same interfacial attractive force and the interfacial repulsive force also occur for dark matter in the opposite direction. Thus, the repulsive MOND force field results in the separation of baryonic matter and dark matter.

The acceleration constant,  $a_0$ , represents the maximum acceleration constant for the maximum incompatibility between baryonic matter and dark matter. The common link between baryonic matter and dark matter is cosmic radiation resulted from the annihilation of matter and antimatter from both baryonic matter and dark matter. With the high concentration of cosmic radiation at the big bang, baryonic matter and dark matter are completely compatible. As the universe ages and expands, the concentration of cosmic radiation decreases, resulting in the increasing incompatibility between baryonic matter and dark matter. The incompatibility reaches maximum when the concentration of cosmic radiation becomes too low for the compatibility between baryonic matter and dark matter. Therefore, for the early universe before the formation of galaxy when the concentration of cosmic radiation is still high, the time-dependent Eq. (42) is as Eq. (48).

$$a_i = \sqrt{\frac{a_N a_0 t}{t_0}} \text{ for } t_0 \geq t, \quad (48)$$

where  $t$  is the age of the universe, and  $t_0$  is the age of the universe to reach the maximum incompatibility between baryonic matter and dark matter.

The distance,  $r_0$ , from the center to the border of the interface is as Eq. (49).

$$r_0 = \sqrt{GM/a_0} \quad (49)$$

In the early universe,  $r_0$  decreases with the age of the universe as Eq. (50).

$$r_0 = \sqrt{\frac{GMt_0}{a_0 t}} \quad (50)$$

The decreases in  $r_0$  leads to the increase in the interface where the interfacial forces exist. The interfacial forces also increase with time.

$a_0 \gg a_i$ , in the interfacial region

$$\begin{aligned} F_{i-R} &= F_{i-A} - F_{i-Newton} \\ &= m \left( \frac{\sqrt{GMa_0 t / t_0}}{r} - \frac{GM}{r^2} \right) \end{aligned} \quad (51)$$

To minimize the interface and the interfacial forces, the same matter materials increasingly come together to form the matter droplets separating from the different matter materials. The increasing formation of the matter droplets with increasing incompatibility is similar to the increasing formation of oil droplets with increasing incompatibility between oil and water. Since there are more dark matter materials than baryonic matter materials, most of the matter droplets are baryonic droplets surrounded by dark matter materials. The early universe is characterized by the increases in the size and the number of the matter droplets due to the increasing incompatibility between baryonic matter and dark matter.

### 3.2. The Formation of the Inhomogeneous Structures

The Inflationary Universe scenario [42] provides possible solutions of the horizon, flatness and formation of structure problems. In the standard inflation theory, quantum fluctuations during the inflation are stretched exponentially so that they can become the seeds for the formation of inhomogeneous structure such as galaxies and galaxy clusters. They also produce anisotropies in CMB (cosmic microwave background).

This paper posits that the inhomogeneous structure comes from both quantum fluctuation during the inflation and the repulsive MOND force between baryonic matter and dark matter after the inflation. As mentioned in the previous section, the increasing repulsive MOND force field with the increasing incompatibility in the early universe results in the increase in the size and number of the matter droplets. At the beginning of the expanding universe after the inflation, baryonic matter existed entirely as free baryonic matter. At the time of the recombination, the inhomogeneous structure by the incompatibility between baryonic matter and dark matter causes small-scale variant in terms of inhomogeneous structure as observed [43] by the presence of small amount of baryonic matter droplets. As the universe expanded after the time of recombination, the density of cosmic radiation decreases, and the size of the baryonic droplets increased with the increasing incompatibility between baryonic matter and dark matter. The growth of the baryonic droplet by the increasing incompatibility from the cosmic expansion coincided with the growth of the baryonic droplet by gravitational instability from the cosmic expansion. The formation of galaxies is through both gravitational instability and the incompatibility between baryonic matter and dark matter.

The pre-galactic universe consisted of the growing baryonic droplets surrounded by the dark matter halos, which connected among one another in the form of filaments and voids. These dark matter domains later became the dark matter halos, and the baryonic droplets became galaxies, clusters, and superclusters.

When there were many baryonic droplets, the merger among the baryonic droplets became another mechanism to increase the droplet size and mass. When three or more homogeneous baryonic droplets merged together, dark matter was likely trapped in the merged droplet (C, D, E, and F in Fig. 10). The droplet with trapped dark matter inside is the heterogeneous baryonic droplet, while the droplet without trapped dark matter inside is the homogeneous baryonic droplet.

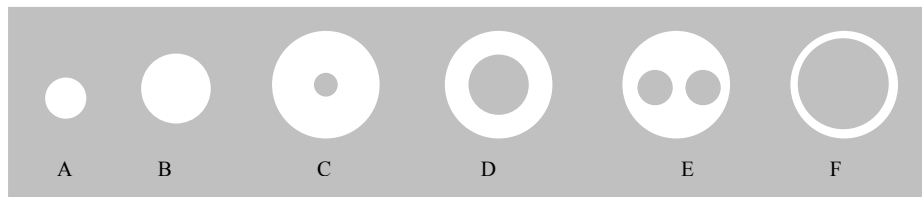


**Fig. 10:** the homogeneous baryonic droplets (A, and B), and the heterogeneous baryonic droplets (C, D, E, and F)

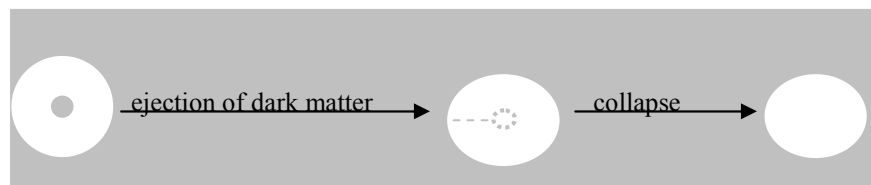
In the heterogeneous droplets C, D, E, and F, dark matter was trapped in the cores of the baryonic droplets. There were the dark matter core, the baryonic matter shell, and the dark matter halo around the baryonic droplet, resulting in two repulsive forces between the dark matter core and the baryonic matter shell and between the baryonic shell and the dark matter halo. When the temperature dropped to  $\sim 1000^{\circ}\text{K}$ , some hydrogen atoms in the droplet paired up to create molecular baryonic matter. The most likely place to form such molecular baryonic matter was in the interior part of the droplet. For heterogeneous droplet, molecular baryonic matter formed a molecular layer around the core. Molecular hydrogen cooled the molecular layer by emitting infrared radiation after collision with atomic

hydrogen. Eventually, the temperature of the molecular layer dropped to around 200 to 300°K, reducing the gas pressure and allowing the molecular layer to continue contracting into gravitationally bound dense molecular layer with high viscosity.

Without electromagnetism, the viscosity of dark matter remained low. The high viscosity in the dense molecular layer around the core restricted the movement of the internal baryon-dark border toward the baryonic matter shell, resulting in restricting the repulsive force between the dark matter core and the baryonic matter shell and in building up the internal pressure in the dark matter core. On the other hand, the low-viscosity dark matter did not hinder the movement of the external baryon-dark border toward the dark matter halo. The increasing difference in the speeds of movement between the internal and external borders increased the fraction of the heterogeneous baryonic droplets.

Subsequently, the whole baryonic matter shell became the dense molecular layer. The dense baryonic matter shell contracted into gravitationally bound clumps, which prevented the movement of the internal border. The dark matter cores build up the high internal pressure from the accumulated droplet repulsive potential. Eventually, the core with high internal pressure caused the eruption to the droplet. The dark matter rushed out of the droplet within a short time, and the baryonic matter shell collapsed. This eruption is much larger in area and much weaker in intensity than supernova. The “big eruption” of the baryonic droplet brings about the different morphologies of galaxies from different types of the baryonic droplets.

If there was small dark matter core as in the heterogeneous baryonic droplet (C in Figure 10), the big eruption involves two steps: the ejection of dark matter from the dark matter core in the center and the collapse of the baryonic droplet. In the first step, when the pressure inside the dark matter core reached a critical point, dark matter rushed out within a short time. As the dark matter core moved out, dark matter stretched the baryonic matter shell, and the baryonic matter shell also stretched in the opposite direction, resulting in elliptical shape in  $E_0$  to  $E_7$  elliptical galaxies, whose lengths of major axes are proportional to the relative sizes of the dark matter core. The ejection of dark matter left behind a void in the center. In the second step, the baryonic matter shell expanded into the void, and the pressure from the external border between external dark matter and the baryonic matter shell caused the collapse of the baryonic droplet. The expansion led to cooling, and the collapse resulted in collision. Cooling and collision produced a shock front of high density in the center, which resulted in the formation of many massive first stars in the center.



It was observed that when the universe was only 3 billion years old, massive star-forming galaxies (SFGs) cranked out at an astonishing rate—25 to 50 times the four solar masses worth of stars the Milky Way currently forms each year. Recently, to account for such astonishing rate of star formation, Dekel and Teyssier [44] postulate that the cold gas streams penetrate through the dark-matter halo of each galaxy and the hot gas that fills it and reach the center, where they become a rotating disk. These disks, each subject

to its own, local, gravitational forces, break into a few giant clumps in which the gas converts into stars very efficiently. They called it Stream-Fed Galaxies (SFG). The incoming baryonic cold stream to the center of galaxy in Stream-Fed Galaxies is similar to the outgoing dark matter leaving the center of baryonic droplet. The expansion of the baryonic matter shell into the void left by dark matter and the collapse of the baryonic droplet generated cooling and collision in the center as in the case of the incoming baryonic cold stream to the center.

After few million years, such massive first stars became supernovas and black holes. Most of the massive first stars became black holes without contributing to the metal enrichment of the surrounding. The mergers of black holes generated the supermassive black hole as the nucleus of quasar. Such first quasar galaxies that occurred as early as  $z = 6.28$  were observed to have about the same sizes as the Milky Way [45].

The supernova shock wave induced the formation of stars in the exterior part of the droplet. The time difference in the formations of the nucleus and the formation of stars in the surface was not large, so there are small numbers of observed young stars in elliptical galaxies. This formation of galaxy follows the monolithic collapse model [46] in which baryonic gas in galaxies collapses to form stars within a very short period. Elliptical galaxies continue to grow slowly as the universe expands.

If the size of the dark matter core is medium (D in Fig. 10), it involves a large change on the baryonic matter shell, resulting in the formation of spiral galaxy. In addition to the ejection of dark matter and the collapse, it involves differential rotation. In the first step, if there was only one opening as an air balloon with one opening, the dark matter stream from the dark matter core and the baryonic stream from the baryonic matter shell moved in opposite directions. Due to the medium size of the matter core, the ejection of dark matter results in much thinner ellipse, almost like a stream. The dark matter stream merges with the surrounding dark matter. The baryonic stream with high momentum penetrated the surrounding dark matter halo. As the baryonic stream penetrated into the dark matter halo, it met resistance from the repulsive force. Eventually, the baryonic stream stopped to advance, and started to rotate.

In the second step, the collapse, the material involved in cooling and collision was much less than the formation of elliptical galaxies, resulting in slower rate of star formation. The third step, the differential rotation, relates to the minimization of the interfacial area due to the incomparability between baryonic matter and dark matter transformed the shape of the stream from linear to disk. (The minimization of the interfacial area is shown in the water bead formation on a wax paper.) To transform into disk shape, the stream underwent differential rotation with the increasing angular speeds toward the center. The fast angular speed around the center allowed the winding of the stream around the center. After few rotations, the structure consisted of a bungle was formed by wrapping the stream at the center and the attached spiral arms as spiral galaxy as Fig. 11.

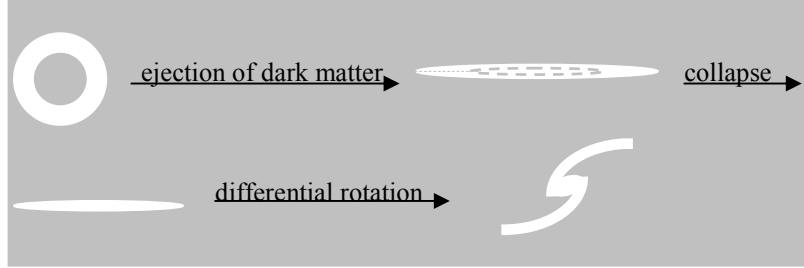


**Fig. 11:** the formation of spiral galaxy

As in elliptical galaxies, the center started the star formation quickly. The low density and high speed of movement in the spiral arm prevented the star formation initially. As the stream wrapped around at the center, the wrapping of the stream produces the high-density region for the star formation in a steady pace. Thus, the first stars and the black holes at the center in spiral galaxies are smaller than in elliptical galaxies. The stars at the center became black holes and supernovas that induced the star formation in spiral arms. The massive center area decreases the angular speed around the center, greatly retarding the winding of the spiral arms around the center. With this steady pace for the star formation, there are still many young stars in spiral galaxies. When there were more than one baryonic stream in the same general direction, there are more than two spiral arms.

Some streams went through the dark matter halos, and entered into the adjacent baryonic droplets. The adjacent droplet captured a part of the stream, and another part of the stream continued to move to the dark matter halo, and finally settled near the droplet in the dark matter halo. Dependent on the direction of the entry, the captured part of the stream later became a part of the disk of the host galaxy, star clusters in the halo, or both. The part of the stream that settled near the droplet became the dwarf spheroidal galaxy. Under continuous disruption and absorption of the tidal interaction from the large galaxy nearby, the dwarf spheroidal galaxy does not have well-defined baryonic-dark border, disk, and internal rotation.

When two dark matter cores inside far apart from each other (E in Fig. 10) generated two openings in opposite sides of the droplet, the dark matter could eject from both openings. In the first step, the two opening is equivalent to the overlapping of two ellipses, resulting in the thick middle part for both the void and the baryonic droplet. As the both ends of the baryonic stream penetrated into the dark matter area, they met resistance from the repulsive force. Eventually, the both ends of the stream stopped, and started to rotate. In the second step, the collapse, cooling and collision took place in the thick middle part of the baryonic droplet, resulting in the star formation in the thick middle part and the formation of barred spiral galaxy. The differential rotation is similar to that of spiral galaxy as Fig. 12.

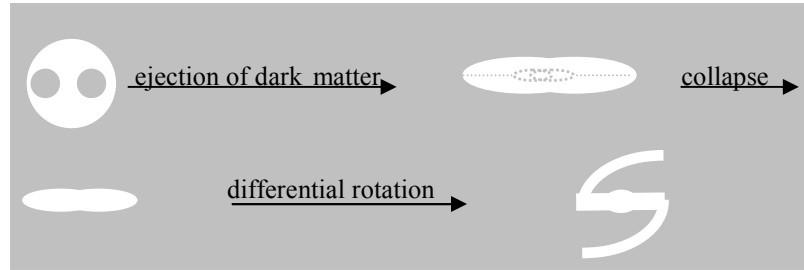


**Fig. 12:** the formation of barred spiral galaxy

The result is barred spiral galaxy. As in normal spiral galaxy, the length of the spiral arm depends on the size of the dark matter core. The smallest dark matter core for barred spiral galaxy brings about SBa, and the largest dark matter core brings about SBd. The stars form in the low-density spiral arms much later than in the nucleus, so they are many young stars in the spiral arms.

If the size of the dark matter core was large (F in Fig. 10), the dark matter core has low internal pressure from the small area of the baryonic matter shell. The escape of the dark matter from the droplet involved little or no eruption, resulting in the gradual migration of large amount of dark matter outward and the gradual migration of small amount of baryonic matter inward. Such opposite migrations are long and continuous processes. The result is irregular galaxy. When enough baryonic matter migrated to the center, and first star formation started. As baryonic matter continues migrating toward the center, the star formation continues in a slow rate up to the present time.

The big rupture explains many puzzling observations of galaxies in the early universe. In the early universe, the galaxies were much more compact than the present nearby galaxies. In the big rupture, the compactness of early galaxies simply is explained by that the star formation started in the center, and gradually spread to outside. As shown earlier, the big rupture provided favorable condition of the observed astonishing rate of star formation. The observation also showed that there was much lower percentage (20%) of the barred spiral universe in the early universe than the observed nearby galaxies (70%). In the big rupture, the total area of two or more dark matter cores led to a larger void in the center for most cases, resulting in the lower density during the collapse, so the rate of star formation for the barred galaxies for most cases was slower. The observed newer barred spiral galaxies are smaller.

At the end of the big eruption, vast majority of baryonic matter was primordial free baryonic matter resided in dark matter outside of the galaxies from the big eruption. This free baryonic matter constituted the intergalactic medium (IGM). Stellar winds, supernova winds, and quasars provide heat and heavy elements to the IGM as ionized baryonic atoms. The heat prevented the formation of the baryonic droplet in the IGM.

Galaxies merged into new large galaxies, such as giant elliptical galaxy and cD galaxy ( $z > 1-2$ ). Similar to the transient molecular cloud formation from the ISM (interstellar medium) through turbulence, the tidal debris and turbulence from the mergers generated the numerous transient molecular regions, which located in a broad area [47]. The incompatibility between baryonic matter and dark matter transformed these transient molecular regions into the stable second-generation baryonic droplets surrounded by the dark matter halos. The baryonic droplets had much higher fraction of hydrogen

molecules, much lower fraction of dark matter, higher density, and lower temperature, and lower entropy than the surrounding.

During this period, the acceleration constant reached to the maximum value with the maximum incompatibility between baryonic matter and dark matter. The growth of the baryonic droplets did not depend on the increasing incompatibility. The growth of the baryonic droplets depended on the turbulences that carried IGM to the baryonic droplets. The rapid growth of the baryonic droplets drew large amount of the surrounding IGM inward, generating the IGM flow shown as the cooling flow. The IGM flow induced the galaxy flow. The IGM flow and the galaxy flow moved toward the merged galaxies, resulting in the protocluster ( $z \sim 0.5$ ) with the merged galaxies as the cluster center.

Before the protocluster stage, spirals grew normally and passively by absorbing gas from the IGM as the universe expanded. During the protocluster stage ( $z \sim 0.5$ ), the massive IGM flow injected a large amount of gas into the spirals that joined in the galaxy flow. Most of the injected hot gas passed through the spiral arms and settled in the bungle parts of the spirals. Such surges of gas absorption from the IGM flow resulted in major starbursts ( $z \sim 0.4$ ) [48]. Meanwhile, the nearby baryonic droplets continued to draw the IGM, and the IGM flow and the galaxy flow continued. The results were the formation of high-density region, where the galaxies and the baryonic droplets competed for the IGM as the gas reservoir. Eventually, the maturity of the baryonic droplets caused a decrease in drawing the IGM inward, resulting in the slow IGM flow. Subsequently, the depleted gas reservoir could not support the major starbursts ( $z \sim 0.3$ ). The galaxy harassment and the mergers in this high-density region disrupted the spiral arms of spirals, resulting in S0 galaxies with indistinct spiral arms ( $z \sim 0.1 - 0.25$ ). The transformation process of spirals into S0 galaxies started at the core first, and moved to the outside of the core. Thus, the fraction of spirals decreases with decreasing distance from the cluster center.

The static and slow-moving second-generation baryonic droplets turned into dwarf elliptical galaxies and globular clusters. The fast moving second-generation baryonic droplets formed the second-generation baryonic stream, which underwent a differential rotation to minimize the interfacial area between the baryonic matter and dark matter. The result is the formation of blue compact dwarf galaxies (BCD), such as NGC 2915 with very extended spiral arms. Since the star formation is steady and slow, so the stars formed in BCD are new.

The galaxies formed during  $z < 0.1-0.2$  are mostly metal-rich tidal dwarf galaxies (TDG) from tidal tails torn out from interacting galaxies. In some cases, the tidal tail and the baryonic droplet merge to generate the starbursts with higher fraction of molecule than the TDG formed by tidal tail alone [49].

When the interactions among large galaxies were mild, the mild turbulence caused the formation of few molecular regions, which located in narrow area close to the large galaxies. Such few molecular regions resulted in few baryonic droplets, producing weak IGM flow and galaxy flow. The result is the formation of galaxy group, such as the Local Group, which has fewer dwarf galaxies and lower density environment than cluster.

Clusters merged to generate tidal debris and turbulence, producing the baryonic droplets, the ICM (intra-cluster medium) flow, and the cluster flow. The ICM flow and the cluster flow directed toward the merger areas among clusters and particularly the rich

clusters with high numbers of galaxies. The ICM flow is shown as the warm filaments outside of cluster [50]. The dominant structural elements in superclusters are single or multi-branching filaments [51]. The cluster flow is shown by the tendency of the major axes of clusters to point toward neighboring clusters [52]. Eventually, the observable expanding universe will consist of giant voids and superclusters surrounded by the dark matter halos.

In summary, the whole observable expanding universe is as one unit of emulsion with incompatibility between baryonic matter and dark matter. The five periods of baryonic structure development are the free baryonic matter, the baryonic droplet, the galaxy, cluster, and the supercluster periods as Fig. 13. The first-generation galaxies are elliptical, normal spiral, barred spiral, irregular, and dwarf spheroidal galaxies. The second-generation galaxies are giant ellipticals, cD, evolved S0, dwarf ellipticals, BCD, and TDG. The universe now is in the early part of the supercluster period.

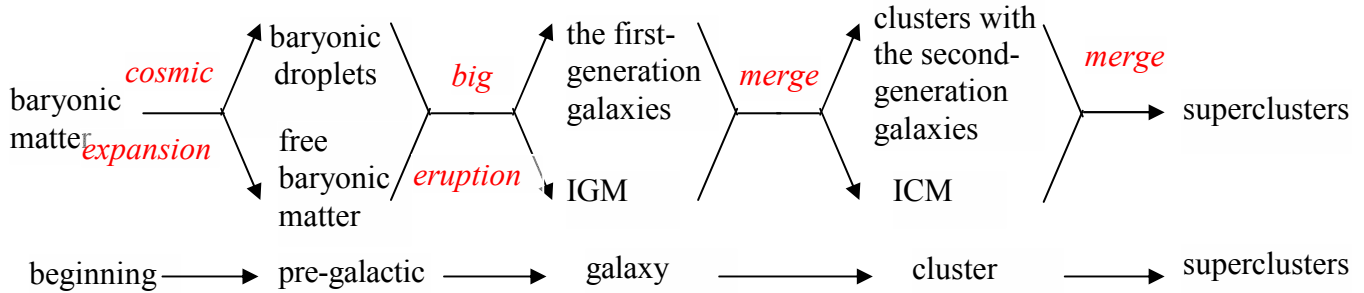


**Fig. 13:** the five levels of baryonic structure in the universe

### 3.3. Summary

The separation of dark matter and baryonic matter involves MOND (modified Newtonian dynamics). It is proposed that the MOND force is in the interface between the baryonic matter region and the dark matter region. In the interface, the same matter materials attract as the conventional attractive MOND force, and the different matter materials repulse as the repulsive MOND force between baryonic matter and dark matter. The source of the repulsive MOND force field is the incompatibility between baryonic matter and dark matter, like water and oil. The incompatibility does not allow the direct detection of dark matter. Typically, dark matter halo surrounds baryonic galaxy. The repulsive MOND force between baryonic matter and dark matter enhances the attractive MOND force of baryonic matter in the interface toward the center of gravity of baryonic matter. The enhancement of the low acceleration in the interface is by the acceleration constant,  $a_0$ , which defines the border of the interface and the factor of the enhancement. The enhancement of the low gravity in the interface is by the decrease of gravity with the distant rather than the square of distance as in the normal Newtonian gravity. The repulsive MOND force is the difference between the attractive MOND force and the non-existing interfacial Newtonian force. The repulsive MOND force field results in the separation and the repulsive force between baryonic matter and dark matter.

The repulsive MOND force field explains the evolution of the inhomogeneous baryonic structures in the universe. Both baryonic matter and dark matter are compatible

with cosmic radiation, so in the early universe, the incompatibility between baryonic matter and dark matter increases with decreasing cosmic radiation and the increasing age of the universe until reaching the maximum incompatibility. The repulsive MOND force field with the increasing incompatibility results in the growth of the baryonic matter droplets. The three periods for the baryonic structure development in the early universe are the free baryonic matter, the baryonic droplet, and the galaxy. The transition to the baryonic droplet generates density perturbation in the CMB. In the galaxy period, the first-generation galaxies include elliptical, normal spiral, barred spiral, irregular, and dwarf spheroidal galaxies.

After reaching the maximum incompatibility, the growth of the baryonic droplets depends on the turbulence, resulting in the baryonic structure development of the cluster and the supercluster. In the cluster period, the second-generation galaxies include modified giant ellipticals, cD, evolved S0, dwarf elliptical, BCD, and tidal dwarf galaxies. The whole observable expanding universe behaves as one unit of emulsion with incompatibility between baryonic matter and dark matter through the repulsive MOND force field.

## 4. The Extreme Force Field

### 4.1. The quantum space phase transitions for force fields

Under extreme conditions such as the absolute zero temperature or extremely high pressure, binary lattice space for a gauge force field undergoes a phase transition to become binary partition space for the extreme force fields [2] [4].

At zero temperature or extremely high pressure, binary lattice space for a gauge force field undergoes a quantum space phase transition to become binary partition space. In binary partition space, detachment space and attachment space are in two separate continuous regions as follows.

$$\begin{array}{ccc}
 \left(1_4\right)_m + \sum_{k=1}^k \left(\left(0_4\right)\left(1_4\right)\right)_{n,k} & \longrightarrow & \left(1_4\right)_m + \sum_{k=1}^k \left(0_4\right)_{n,k} \left(1_4\right)_{n,k} \\
 \textit{particle boson field} & & \textit{extreme particle extreme boson field} \\
 \textit{in binary lattice space} & & \textit{in binary partition space}
 \end{array} \quad (52)$$

The force field in binary lattice space is gauge boson force field, the force field in binary partition space is denoted as “extreme boson force field”. The detachment space in extreme boson field is the vacuum core, while extreme bosons attached to attachment space form the extreme boson shell. Gauge boson force field has no boundary, while the attachment space in the binary partition space acts as the boundary for extreme boson force field. Extreme boson field is like a bubble with core vacuum surrounded by membrane where extreme bosons locate.

The overlapping (connection) of two extreme bosons from two different sites results in “extreme bond”. The product is “extreme molecule”. An example of extreme molecule is Cooper pair, consisting of two electrons linked by extreme bond. Another example is superfluid, consisting of molecules linked by extreme bonds. Extreme bonds can be also formed among the sites in a lattice, resulting in extreme lattice. Extreme lattice is superconductor. Extreme boson force is incompatible to gauge boson force field. The incompatibility of extreme boson force field and gauge boson force field manifests in the Meissner effect, where superconductor (extreme lattice) repels external magnetism. The energy (stiffness) of extreme boson force field can be determined by the penetration of boson force field into extreme boson force field as expressed by the London equation for the Meissner effect.

$$\nabla^2 H = -\lambda^{-2} H \quad , \quad (53)$$

where H is an external boson field and  $\lambda$  is the depth of the penetration of magnetism into extreme boson shell. This equation indicates that the external boson field decays exponentially as it penetrate into extreme boson force field.

## 4.2. Superconductor and the Fractional Quantum Hall Effect

Extreme boson exists only at the absolute zero temperature. However, quantum fluctuation at a temperature close to zero temperature allows the formation of an extreme boson. The temperature is the critical temperature ( $T_c$ ). Such temperature constitutes the quantum critical point (QCP) [ 53 ]. Extreme boson at QCP is the base of superconductivity.

The standard theory for the conventional low temperature conductivity is the BCS theory. According to the theory, as one negatively charged electron passes by the positively charged ions in the lattice of the superconductor, the lattice distorts. This in turn causes phonons to be emitted which forms a channel of positive charges around the electron. The second electron is drawn into the channel. Two electrons link up to form the "Cooper pair" without the normal repulsion.

In the extreme boson model of the BCS theory, an extreme boson instead of a positive charged phonon is the link for the Cooper pair. According the extreme boson model, as an electron passes the lattice of superconductor, lattice atom absorbs the energy of the passing electron to cause a lattice bond to stretch or to contract. When the lattice bond recoils to normal position, the lattice atom emits a phonon, which is absorbed by the electron. The electron then emits the phonon, which is absorbed by the next lattice atom to cause its bond to stretch. When the lattice bond recoils to normal position, the lattice atom emits a phonon, which is absorbed by the electron. The result is the continuous lattice vibration by the exchanges of phonons between the electrons in electric current and the lattice atoms in lattice.

At the temperature close to the absolute zero temperature, the lattice vibration continuously produces phonons, and through quantum fluctuation, a certain proportion of phonons converts to extreme bosons. Extreme bonds are formed among extreme bosons, resulting in extreme lattice. At the same time, the electrons involved in lattice vibration form extreme molecules as Cooper pairs linked by extreme bonds. Such extreme bond excludes electromagnetism, including the Coulomb repulsive force, between the two electrons. When Cooper pairs travel along the uninterrupted extreme bonds of an extreme lattice, Cooper pairs experience no resistance by electromagnetism, resulting in zero electric resistance. Extreme lattice repels external magnetism as in the Meissner effect.

The extreme bosons involved in the formation of the extreme lattice bonds and the extreme molecular bonds have the energy, so the extreme bond energy ( $E_l$ ) for the extreme lattice is same as the extreme bond energy ( $E_c$ ) for Cooper pair.

$$\begin{aligned} E_l &= E_c \\ &= 2\Delta_0 \end{aligned} \tag{54}$$

The extreme bond energy corresponds to two times the energy gap  $\Delta_t$  at zero temperature in the BCS theory. The energy gap is the superconducting energy that an electron has.  $\Delta_t$  approaches to zero continuously as temperature approaches to  $T_c$ . The elimination of superconductivity is to break the extreme bonds of the extreme lattice and Cooper pairs.

Extreme boson force is a confined short distant force, so the neighboring extreme bosons have to be close together. To have a continuous extreme lattice without gaps, it is

necessary to have sufficient density of the vibrating lattice atoms. Thus, there is critical density,  $D_c$ , of vibrating lattice atoms. Below  $D_c$ , no extreme lattice can be formed. In a good conductor, an electron hardly interacts with lattice atoms to generate lattice vibration for extreme boson, so a good conductor whose density for vibrating lattice atoms below  $D_c$  does not become a superconductor.  $T_c$  is directly proportional to the density of vibrating lattice atoms and the frequency of the vibration (related to the isotope mass).

The “gap” in extreme lattice is the area without vibrating lattice atoms. The gap allows electric resistance. Superconductor has “perfect extreme lattice” without significant gap, while “imperfect extreme lattice” has significant gap to prevent the occurrence of superconductivity.

High temperature superconductor has a much higher  $T_c$  than low temperature superconductor described by the BCS theory. All high temperature superconductors involve the particular type of insulator with various kinds of dopants. A typical insulator is Mott insulator, such as copper oxides,  $\text{CuO}_2$ .  $\text{CuO}_2$  forms a two-dimensional layer, with the Cu atoms forming a square lattice and O atoms between each nearest-neighbor pair of Cu atoms. In the undoped  $\text{CuO}_2$ , all of the planar coppers are in the  $\text{Cu}^{2+}$  state, with one unpaired electron per site. Two neighboring unpaired electrons with antiparallel spins have lower ground energy than two neighboring unpaired electrons with parallel spins. Two neighboring unpaired electrons with antiparallel spins constitute the antiparallel spin pair, which has lower ground state energy than the parallel spin pair. Consequently,  $\text{CuO}_2$  layer consists of the antiparallel spin pairs, resulting in antiferromagnetism.

The insulating character of this state is thought to result, not from the antiferromagnetism directly, but from the strong on-site Coulomb repulsion, which is the energy cost of putting an extra electron on a Cu atom to make  $\text{Cu}^{1+}$ . This Coulomb energy for double occupancy suppresses conduction.

$\text{La}_x \text{Sr}_x \text{Cu}_2 \text{O}_4$  is an example of high temperature conductor. The key ingredient consists of  $\text{CuO}_2$  layers. The doping of Sr provides chemical environment to shift the charge away from the  $\text{CuO}_2$  layers, leaving “doping holes” in the  $\text{CuO}_2$  layers. The shifting of electrons allows the occurrence of electric current. In the t-J model of high temperature superconductor, an electron in electric current is fractionalized into two fractional electrons to carry spin quantum number in t and to carry charge in J [54].

$$H_{ij} = -t \sum_{ij\sigma} \tilde{c}_{i\sigma}^+ \tilde{c}_{j\sigma} + J \sum_{ij} \left[ \vec{s}_i \cdot \vec{s}_j - \frac{n_i n_j}{4} \right], \quad (55)$$

In the extreme boson model, t corresponds to the spin current (spinon) to generate spin fluctuation in the metal oxide layer, while J corresponds to the directional charge current (phonon as in the BCS theory) along the metal oxide layers. Extreme boson force field is a confined force field. As long as electrons are in the confined extreme boson force field, it is possible to have fractionalized electrons, similar to the fractionalized charges of quarks in the gluon force field.

The spin fluctuation generated by the spin current in the layer comes from doping holes in CuO<sub>2</sub> layer. When an antiparallel spin pair loses an electron by doping, a doping hole is in the spin pair. The adjacent electron outside of the pair fills in the hole. The filled-in electron has a parallel spin as the electron in the original pair. Parallel spin pair has higher ground state energy than antiparallel pair, so the filled-in electron absorbs a spinon to gain enough energy to undergo a spin change. The result is the formation of an antiparallel spin pair. The antiparallel spin pair has lower ground state energy than an antiparallel spin pair, so it emits a spinon. After the electron fills the hole, the hole passes to the next adjacent pair. The next adjacent pair then becomes the next adjacent newly formed parallel pair, which then absorbed the emitted spinon undergo spin change to form an antiparallel spin pair. The continuous passing of holes constitutes the layer spin current. The layer spin current throughout the CuO<sub>2</sub> layer generates the continuous spin fluctuation [55] with continuous emission and absorption of spinons.

At a low temperature, the spin fluctuation continuously produces spinons, and through quantum fluctuation, a certain proportion of spinons converts to extreme bosons. Extreme bonds are formed among extreme bosons. The extreme bonds are the parallel extreme bonds parallel to CuO<sub>2</sub> layer. The parallel extreme bond results from the spin current.

The extreme bonds connecting CuO<sub>2</sub> layers are the perpendicular bonds perpendicular to CuO<sub>2</sub> layers through d-wave by the lattice vibration, like the lattice vibration in the low temperature superconductor. The perpendicular bond results from the charge current. The perpendicular extreme bond energy ( $E_{\perp}$ ) is greater than the parallel extreme bond energy ( $E_{\parallel}$ ). Cooper pairs as the charge pairs travel along the perpendicular bonds. Thus, Cooper pair has the same bond as the perpendicular extreme bond. The extreme lattice consists of both parallel extreme bonds and perpendicular extreme bonds.

$$\begin{aligned} E_{II} &< E_{\perp} \\ E_c &= E_{\perp} \\ E_I &= E_{\parallel, \perp} \end{aligned} \quad , \quad (56)$$

Perfect extreme lattice without gap of extreme bonds consists of both perfect parallel extreme lattice and perfect perpendicular extreme lattice without gaps for parallel extreme bonds and perpendicular bonds, respectively. The  $T_c$  of high temperature superconductor the transition temperature to the perfect extreme lattice, consisting of the perfect parallel extreme lattice and the perfect perpendicular lattice. Because many extreme bosons are generated from many spin fluctuations,  $T_c$  is high.

Having stronger extreme bond, the  $T_{c\perp}$  for the perpendicular extreme lattice is higher than the  $T_{c\parallel}$  for the parallel extreme lattice. Thus,  $T_c$  for the extreme lattice is essentially the  $T_{c\parallel}$  for the parallel extreme lattice.

$$T_{cII} < T_{c\perp}$$

$$T_c = T_{cII} \quad , \quad (57)$$

There are five different phases of metal oxide related to the presence or the absence of perfect parallel lattice, perfect perpendicular extreme lattice, and Cooper pairs as follows.

**Table 4.** The Phases of Metal Oxides

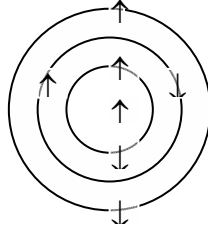
Phase/structure	perfect parallel extreme lattice for spinons	perfect perpendicular extreme lattice for phonons	Cooper pair
Insulator	no	no	no
Pseudogap	no	yes	yes
Superconductor	yes	yes	yes
non-fermi liquid	no	no	yes
normal conductor	no	no	no

Without doping, metal oxide is an insulator. The pseudogap phase has a certain amount of doping. With a certain amount of doping, the perfect perpendicular extreme lattice can be established with the pseudogap transition temperature,  $T_p$ , equal to  $T_{c\perp}$ . However, the parallel lattice is imperfect with gaps, so it is not a superconductor. The pseudogap phase can also be achieved by the increase in temperature above  $T_c$  to create gap in the parallel extreme lattice, resulting in imperfect parallel extreme lattice. Different points in the pseudogap phase represent different degrees of the imperfect parallel extreme lattice. With the optimal doping, the pseudogap phase becomes the superconductor phase below  $T_c$ . Superconductor has perfect parallel extreme lattice and perfect perpendicular extreme lattice. With excessive doping, the superconductor phase becomes the conductor phase without significant spin fluctuation and lattice vibration. In the non-fermi liquid region, the extreme lattice is imperfect by the combination of the moderate increase in temperature above  $T_c$  and the moderate increase in doping. However, non-fermi liquid phase still has Cooper pairs that do not require the presence of perfect extreme lattice. In the non-fermi liquid phase, due to the breaking of Cooper pairs with the increase in temperature, the transport properties are temperature dependent, unlike normal conductor.

In summary, for a low-temperature superconductor, extreme bosons are generated by the quantum fluctuation in lattice vibration by the absorption and the emission of phonons between passing electrons and lattice atoms. The connection of extreme bosons results in extreme lattice and Cooper pairs. For a high-temperature superconductor, extreme bosons are generated by the quantum fluctuation in spin fluctuation and lattice vibration by the absorption and the emission of spinons and phonons, respectively. The extreme lattice consists of the parallel extreme bonds and the perpendicular extreme bonds. Because many extreme bosons are generated from many spin fluctuations,  $T_c$  is high.

The extreme boson can also explain the fractional quantum Hall effect (FQHE) [56] [57]. In the FQHE, electrons travel on a two-dimensional plane. In two-dimensional systems, the electrons in the direction of the Hall effect are completely separate, so the extreme bond cannot be formed between the electrons. However, an individual electron can have n extreme bosons from the quantum fluctuation of the magnetic flux at a very low temperature, resulting in extreme atom that consists of an electron and n extreme bosons with n extreme boson force fields.

Extreme boson force field consists of a core vacuum surrounded by only one extreme boson shell. An electron can be in  $n \geq 1$  extreme boson force fields. If  $n = 1$ , an electron in a extreme boson force field delocalizes to the extreme boson shell, resulting in the probability distribution in both the center and the boson shell denoted as the extreme atomic orbital. (Unlike extreme boson force field, gauge boson force field can have infinitive number of orbitals.) The probability distribution fractionalizes the electron into one fractional electron at the center and the  $2p$  fractional electron in the extreme atomic orbital. Thus, the extreme atom ( $n = p = 1$ ) has three fractional electrons, and each fractional electron has  $-1/3$  charge. For  $n > 1$ , the multiple extreme force fields are like multiple separate bubbles with one fractional electron at the center. For  $p = 1$  and  $n = 3$ , the total number of fractional electrons is 7, and each fractional electron has  $-1/7$  charge as follows.



The formulas for the number of fractional electrons and fractional charge are as follows.

$$\begin{aligned} \text{number of fractional electrons} &= 2pn + 1 \\ \text{electric charge} &= -1 / (2pn + 1) \end{aligned} \quad , \quad (58)$$

where  $n$  = the extreme atomic orbital number and  $2p$  = number of fractional electrons per orbital. The wavefunction of the extreme atom is as follows.

$$\Psi_n = \Phi \sum_n \left( \prod_{j < k} (z_j - z_k)^{2p} \right)_n \quad , \quad (59)$$

where  $\Phi$  is for the fractional electron at the center,  $z_j = x_j - iy_j$ ,  $n$  = number of extreme atomic orbital, and  $2p$  = number of fractional electrons per orbital. For the integer quantum Hall effect,  $p = n = 0$ . Eq. (59) is an electron in one or multiple extreme boson force fields. The probability distribution fractionalizes the electrons into the  $k$  fractional electron at the center ( $\Phi$ ) and the  $2p$   $j$  fractional electrons in the extreme atomic orbital. In Eq. (59), the  $j$  fractional electron in the extreme atomic orbital takes a loop around the

k fractional electron at the center. One extreme boson force field can have only one extreme atomic orbital. When the electron is in multiple n extreme boson force fields, there are n separate extreme atomic orbitals with different sizes.

This wavefunction is same as same as the wavefunction of the composite fermion, which consists of an electron and 2p flux quanta [58]. In the composite fermion,  $\Phi$  is the non-interacting electron and 2p is the number of flux quanta. The composite fermion is the bound state of an electron and 2p quantum vortices. In the same way, the extreme atom is the bound state of a fractional electron and 2pn fractional electrons in the extreme atomic orbitals. The extreme atomic orbital can be also described by the Laughlin-Jastrow factor by counting the centered fractional electron as a part of the extreme atomic orbital electrons, resulting in odd number of quasiparticles.

The extreme atoms provide the ground state for the Landau level. Within the ground state, the extreme atom with higher n and p has higher energy and lower probability. During the generation of the Landau levels, the fractional electrons come off the extreme atomic orbitals. The most favorable way is to remove one fractional electron per extreme atomic orbital to provide more room for the other fractional electron in the same extreme atomic orbital. For n =1, one -1/3 charged electron comes off. For n = 2, two -1/5 charged electrons come off. The formula is  $-n / (2n+ 1)$  electric charge as observed: -1/3, -2/5, -3/7... [59]. The second series is the leftover of the first series: -2/3, -3/5, -4/7...

### 4.3. Gravastar, Supernova, Neutron Star, and GRB

Black hole has been a standard model for the collapse of a supermassive star. Two alternates for black hole are gravastar [60] [61] and dark energy star [62]. Gravastar is a spherical void as Bose-Einstein condensate surrounded by an extremely durable form of matter. For dark energy star, the mass-energy of the nucleons under gravitational collapse can be converted to vacuum energy. The negative pressure associated with a large vacuum energy prevents the formation of singularity and results in an explosion. This paper proposes gravastar based on extreme boson field.

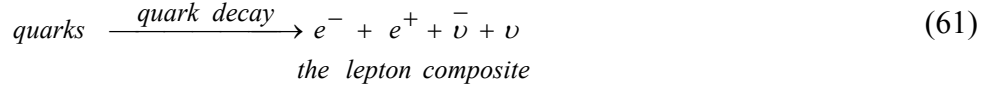
Before the gravitational collapse of large or supermassive star, the fusion process in the core of the star to create the outward pressure counters the inward gravitational pull of the star's great mass. When the core contains heavy elements, mostly iron, the fusion stops. Instantly, the gravitational collapse starts. The great pressure of the gravity collapses atoms into neutrons. Further pressure collapses neutrons to quark matter and heavy quark matter.

Eventually, the high gravitational pressure transforms the gauge gluon force field into the extreme gluon force field, consisting of a vacuum core surrounded by an extreme gluon shell, like a bubble. The exclusion of gravity by the extreme gluon force field as in the Meissner effect prevents the gravitational collapse into singularity. In the Meissner effect for superconductor, a very strong magnetism can collapse the extreme boson force field, resulting in the disappearance of superconductivity. Superconductivity is based on quantum fluctuation between the gauge boson force field and the extreme boson force field, so it is possible to collapse the extreme boson force field. The formation of the extreme gluon force field is not by quantum fluctuation, so the extreme gluon force field cannot be collapsed. To keep the extreme gluon force field from collapsing, the vacuum

core in the extreme gluon force field acquires a non-zero vacuum energy whose density ( $\rho$ ) is equal to negative pressure ( $p$ ). The space for the vacuum core becomes de Sitter space. The vacuum energy of the vacuum core comes from the gravitons in the exterior region surrounding the extreme gluon force field as in the Chapline's dark energy star. The external region surrounding the extreme gluon force field becomes the vacuum exterior region. Thus, the core of gravastar can be divided into three regions: the vacuum core, the extreme gluon shell, and the vacuum exterior region.

$$\begin{aligned}
 \text{vacuum core region} &: \rho = -p \\
 \text{hedge gluon shell region} &: \rho = +p \quad , \\
 \text{vacuum exterior region} &: \rho = p = 0
 \end{aligned}
 \tag{60}$$

Quarks without the strong force field are transformed into the decayed products as electron-positron and neutrino-antineutrino denoted as the "lepton composite".



The result is that the core of the collapsed star consists of the lepton composite surrounded by the extreme gluon field. This lepton composite-extreme gluon force field core (LHC) constitutes the core for gravastar. The star consisting of the lepton composite-extreme gluon field core (LHC) and the matter shell is "gravastar". The matter shell consists of different layers of matters: heavy quark matter layer, quark matter layer, neutron layer, and heavy element layer one after the other.

**LHC** (*lepton composite – hedge gluon force field core*):

$$\begin{aligned}
 \text{lepton composite region} &: \rho = +p \\
 \text{vacuum core region} &: \rho = -p \\
 \text{hedge gluon shell region} &: \rho = +p \\
 \text{vacuum exterior region} &: \rho = p = 0
 \end{aligned}$$

**Matter Shell**:  $\rho = +p$

*heavy quark layer*  
*quark layer*  
*neutron layer*  
*heavy element layer*

(62)

The standard theory for supernova is that neutrinos released from nuclear fusion provide the energy needed to blow off the stellar mantle in a supernova, but details calculation shows that the neutrinos are too few and too weakly interacting for the required explosion [63].

In the extreme boson model, supernova is the lepton composite-powered exploding gravastar. The progenitor of supernova is a large star. The collapse of the star forms a gravastar with the LHC and the matter shell. Immediately after the formation of the gravastar, the matter shell derived from a large star does not have strong enough gravity to prevent the cracking of the matter shell by the outward pressure of the LHC. Through the cracks, the escaping lepton composite from the core becomes the “relativistic lepton composite” by adding kinetic energy converted from the non-zero vacuum energy of the extreme gluon force field. The relativistic lepton composite through the cracks explodes the heavy element layer of the matter shell, where gravity is weaker, and the crack is larger. The explosion is nearly symmetrical.

The inner part of the matter shell then collapses to form neutron star as the core remnant of supernova. The collapse of star initiates the rotation for neutron star with magnetic field. Pulsar is the rotational neutron star that contains a small remnant of the LHC after supernova.

The LHC remnant is large enough to crack the pulsar slightly. Through the small cracks, relativistic lepton composite leaks out continuously, and carries neutrons on the wall of the cracks to the surface of the magnetized rotational pulsar. The neutrons brought out by the relativistic lepton composite are highly energetic. These energetic neutrons quickly decay into protons and electrons, which rotate in the magnetic field. The energy that the particles carry by relativistic lepton composite accelerates the rotation of the pulsar. The rotating particles accelerate to the speeds approaching to the speed of light, resulting in synchrotron emission. The radiation is released as intense beams from the magnetic poles of the pulsar. The emitted radiation beam is rotated and sweeps regularly past the earth with precise period. The primary power source of the emitted radiation from pulsar is the relativistic lepton composite, not the magnetic field. Therefore, a slow-rotating pulsar with a weak magnetic field can still maintain the emitted radiation.

The progenitor star of magnetar is much larger than the progenitor of an ordinary pulsar. During the supernova explosion, the high gravity of the large remnant neutron star attracts the debris to fall back on the remnant neutron star. The falling debris, mostly heavy elements, penetrates the remnant neutron star to form embedded heavy elements. The amount of embedded heavy elements increases with increasing mass with increasing gravity of the progenitor star. Since the progenitor of magnetar is large, it has large amount of embedded heavy elements, weakening its structure, and causing large relativistic lepton composite-powered cracks in the matter shell. Large crack allows the release of high amount of relativistic lepton composite, so the emitted radiation includes high-energy X-ray from minor cracks and occasionally gamma ray burst from major cracks. Because of larger cracks, the disappearance of emitted radiation due to the disappearance of the relativistic lepton composite is quicker than ordinary pulsar.

The progenitor of GRB is a supermassive gravastar with millions sun masses. The matter shell in supermassive gravastar has strong enough gravity to prevent the cracks to disintegrate the matter shell by the outward pressure of the LHC. However, because of the outward pressure from the LHC, the supermassive gravastar is susceptible to crack by impact. The matter shell consists of the heavy quark matter layer, quark matter layer, neutron layer, and heavy element layer. Because of its large size, it has a large heavy element layer as the outer layer.

The GRB results from the volcano eruption initiated by the impact of a neutron star on a supermassive gravastar. The falling of a neutron star through the gravitational field of a gravastar generates high heat on the surface of the neutron star. Upon the impact, the heat of the neutron star liquefies the heavy elements on the surface of the gravastar into the “heavy element ocean”. The heat on the surface of the neutron star dissipates by the liquefaction. Then, the momentum of the neutron star breaks the heavy elements into large pieces, denoted as the “heavy element balls”. Finally, it reaches the neutron layer of the gravastar. The impact breaks the neutron star into large pieces, denoted as “the neutron balls”. The impact generates cracks into the LHC. Because of the extremely high gravity of the supermassive gravastar, all balls and liquid heavy elements are kept on the surface of the gravastar. Thus, the impact generates three layers (the heavy element ocean, the heavy element balls, and the neutron balls) and the cracks into the LHC.

Through the cracks generated by the impact, the escaping relativistic lepton composite through the cracks provides the kinetic energy to start the gravastar volcano eruption. First, the relativistic lepton composite carries the “heavy element material” (HEM) in the heavy element ocean in the form of the HEM jets to escape the gravity of the gravastar. There are many separated jets from many different cracks in a broad area, so it is a widespread volcano eruption. Soon, the heavy element ocean is almost dry.

At the same time, the flow of the relativistic lepton composite enlarges the cracks, resulting in increasing flow rate. The high flow rate of the relativistic lepton composite provides enough kinetic energy to carry the heavy element balls to escape the gravity of the gravastar. Each escaping ball has to have enough kinetic energy to escape from the gravity, so each jet can eject one heavy element ball in the interval of few minutes. The escaping HEM forms the HEM band outside of the gravastar, while the heavy element balls form the heavy element ball band. At this time, the relativistic lepton composite is not strong enough to accelerate them to relativistic velocity. They remain non-relativistic. The HEM band eventually merges with the interstellar medium (ISM) to form a very thick layer of the HEM-ISM band.

The flow of the relativistic lepton composite further enlarges the cracks to increase the flow rate of the relativistic lepton composite. Eventually, the flow rate of the relativistic lepton composite is high enough to provide the kinetic energy for the neutron balls to escape the gravity of the gravastar. Each escaping ball has to have enough kinetic energy to escape from the gravity, so each jet can eject one neutron ball in the interval of few minutes. The neutron balls at this time are non-relativistic with the distance of few minutes between the adjacent neutron balls from the same jet. The escaping neutron balls form the neutron ball band.

Finally, the cracks are large enough to allow a huge amount of the relativistic lepton composite to eject from the volcano as the relativistic lepton composite jets. The relativistic lepton composite jets form the relativistic jet band. The initial ejecta composition is as in Fig, 14.

## The Gravastar Volcano Eruption

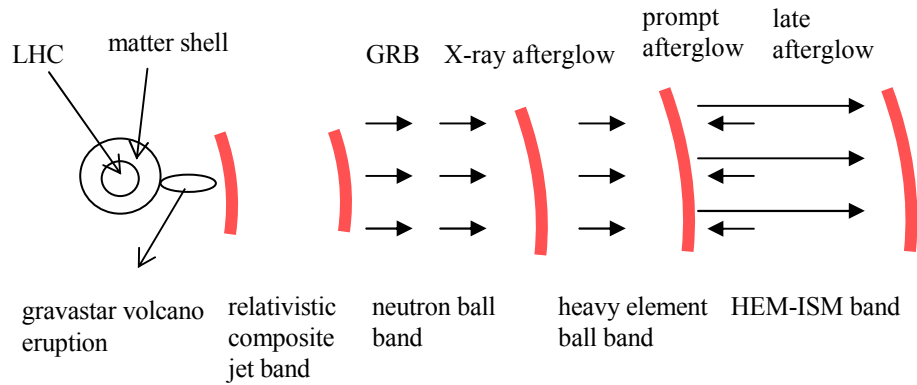


**Fig. 14:** The initial ejecta consist of the HEM-ISM band, the heavy element ball band, the neutron ball band, and the relativistic lepton composite jet band. The merges of various bands produce the GRB, the X-ray afterglow, the prompt afterglow, and the late afterglow in different regions.

The relativistic lepton composite jets sweep through all bands. The chance of being hit by the relativistic lepton composite jets decreases with the distance from the volcano. The majority of the relativistic jets accelerate the neutron balls to relativistic velocity, resulting in the relativistic neutron balls. The synchrotron emission by the acceleration from the relativistic neutron balls brings about the GRB. The acceleration of each neutron ball represents one burst. In the terms of the fireball model [64] [65], the relativistic lepton composite jet corresponds to the baryon-free fireball providing the kinetic energy for the internal and external shocks.

The volcano eruption depletes the relativistic lepton composite in a gravastar. Eventually, the pressure from the depleted source of the relativistic lepton composite becomes too low to prevent the collapse of the cracks by the gravitational pressure in the interior part of gravastar. The emission of the relativistic lepton composite through the volcano starts to decline sharply. Finally, all interior cracks collapse, and the major volcano eruption stops. The major volcano eruption lasts from 2 seconds to few minutes. (The high gravitational pressure replenishes the lepton composite afterward.) However, the volcano continues to eject the residual relativistic lepton composite as the weak residual relativistic lepton composite jets for few hours to few days. The weak residual relativistic lepton composite jets are not strong enough to cause further GRB.

After the stop of the major volcano eruption, the relativistic neutron balls start to collide with the non-relativistic neutron balls ahead. The closest non-relativistic neutron ball is few minutes ahead as the interval for the ejection of neutron ball during the volcano eruption. The collision between the relativistic neutron ball and the non-relativistic neutron ball leads to the deceleration, resulting in the synchrotron emission for the X-ray afterglow.

During the major volcano eruption, when the volcano ejects the neutron balls, the relativistic lepton composite enlarges not only the cracks vertically to the LHC but also the cracks in the heavy element layer on the shore of the heavy element ocean horizontally. After while, the flow rate of the relativistic lepton composite is high enough to eject large pieces of heavy element material on the shore of the ocean as the heavy

element balls. These ejected heavy element balls are off-centered from the center where the neutron balls are ejected. Thus, the volcano ejects the off-centered heavy element balls along with the centered neutron balls in the late stage of the neutron ball ejection. The off-centered heavy element balls accelerated by the relativistic lepton composite jets become the off-centered relativistic heavy element balls. The density and the mass of the neutron ball are high, so the velocity of the relativistic neutron ball is lower than the relativistic heavy element ball. The off-centered heavy element balls occur later than the centered neutron balls, so the number of the heavy element balls is lower than the number of the neutron balls, resulting in the lower number density of the off-centered heavy element balls than the centered neutron balls.

As results, the centered relativistic neutron balls have lower velocity and higher number density than the off-centered relativistic heavy element balls. After the stop of the major volcano eruption, the low number density and off-centered heavy element balls collide first with the non-relativistic balls in the off-centered area of the neutron ball band. Because of the low number density, the slope for the number of collision is steep. Then, the centered relativistic neutron balls collide with the non-relativistic balls in the centered area of the neutron ball band. Because of the high number density, the slope for the number of collision is shallow.

The remaining relativistic balls without collisions in the neutron ball band collide with the non-relativistic balls in the heavy element ball band. These off-centered faster relativistic heavy element balls collide before the centered slower relativistic neutron balls. Therefore, there are four different types of collisions to produce X-ray afterglow in the four different time periods as shown in Fig. 15.

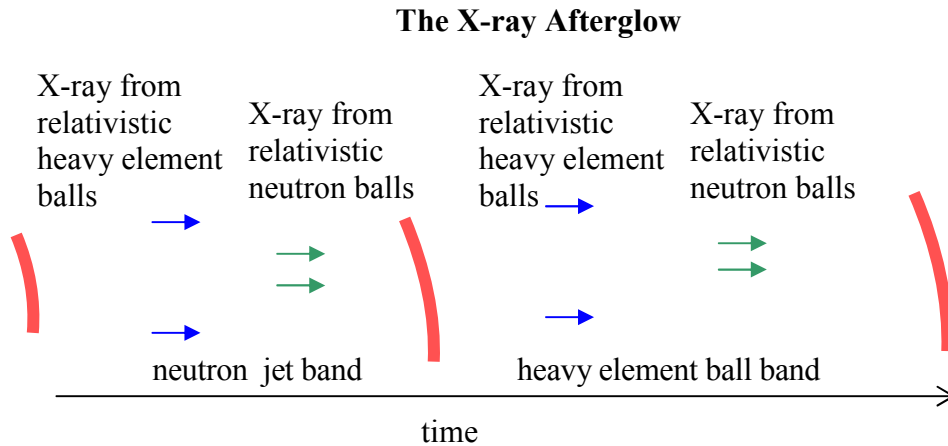


**Fig. 15:** There are the four types of the collisions to generate the X-ray afterglow in the order of occurrences. The first one is the collisions between the off-centered relativistic heavy element balls and the non-relativistic balls. The second one is the collisions between the centered relativistic neutron balls and the non-relativistic balls. The third one is the off-centered relativistic heavy element balls and the non-relativistic balls. The fourth one is the centered relativistic neutron balls and the non-relativistic balls.

The time periods overlap, but in a certain time period (especially the first and the second periods), one type of collisions dominates. They are the four distinct regions for the four different types of collisions as in the observed X-ray lightcurve [66]. A brief renewing of the volcano eruption during the early part of the X-ray afterglow accelerates the balls to bring about a sharp increase of X-ray emission (X-ray flare) from the synchrotron emission.

The leftover relativistic lepton composite from the collisions with the balls is the free relativistic lepton composite, which has considerable lower intensity than the relativistic lepton composite in the origin relativistic lepton composite jets. It reaches the HEM-ISM band slightly ahead the GRB that requires time for acceleration. The thick HEM-ISM reflects considerable amount of relativistic lepton composite as the “reverse shock” traveling backward. Soon after, the stop of the major volcano eruption causes the steep decline in the intensity of the relativistic lepton composite, so for a short time, the strong reverse shock traveling backward dominates the weak “forward shock” from the relativistic lepton composite under steep decline in intensity, resulting in a net reverse shock. The net reverse shock is followed by the weak forward shock from the weak residual relativistic lepton composite jets for few hours to few days as shown in Fig. 16.

### The Net Reverse Shock and the Net Forward Shock

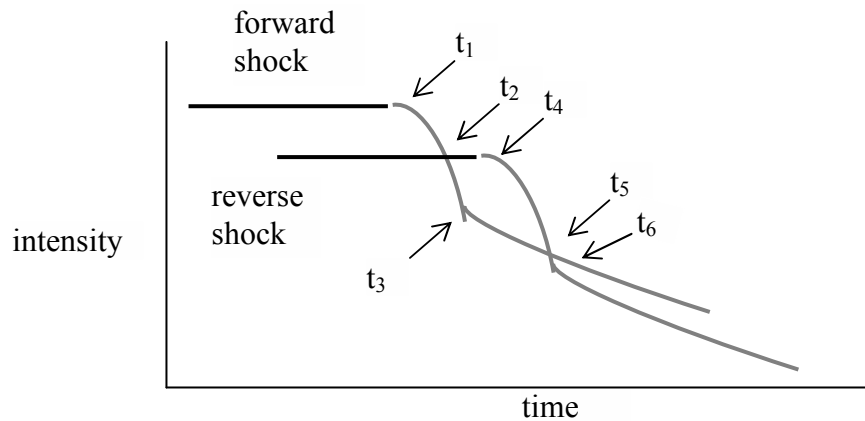


**Fig. 16:** The top curve is the intensity-time curve for the forward shock, and the bottom curve is the identical curve with lower intensity and later time for the reverse shock.  $t_1$  = the start of the end of the eruption,  $t_2$  = the start for the net reverse shock,  $t_3$  = the start of the residual relativistic lepton composite jet,  $t_4$  = the peak for the net reverse shock,  $t_5$  = the end for net reverse shock and the start for the net forward shock, and  $t_6$  = the peak for the net forward shock

In Fig. 16, the top curve is the intensity-time curve for the forward shock, and the bottom curve is the identical curve with lower intensity and later time for the reverse shock. At  $t_1$ , the eruption starts steep decline. At  $t_2$ , the net reverse shock starts to appear. At  $t_3$ , the residual relativistic lepton composite jet starts. At  $t_4$ , the net reverse shock reaches the peak. At  $t_5$ , the net reverse shock disappears, and the net forward shock starts to appear. At  $t_6$ , the net forward shock reaches the peak followed by the decline in

intensity from the continuously declining residual relativistic lepton composite jets. Therefore, both the net reverse shock and the net forward shock have peaks in the intensity-time curves.

The main emissions for the net reverse shock and the net forward shock are the HEM-ISM emissions by the shocks. The emissions are the prompt afterglow by the net reverse shock and the late afterglow by the net forward shock. They are mostly UV, optical, IR, and radio wave. The net reverse shock has lower frequency than the net forward shock due the reduction of frequency during the reflection, so the prompt afterglow has lower frequency emissions than the late afterglow.

If the net reverse shock is in region of the HEM-ISM band far away from the heavy element ball band, the net reverse shock sweeps the region in the HEM-ISM band to generate emissions from the HEM-ISM. Then, the net forward shock sweeps the same region to generate emissions from the HEM-ISM. In this case, the only factor involved in the lightcurves is their intensity-time curves with two distinct peaks in agreement with the observation [65]. It is categorized as the “re-brightening” type with two distinctive peaks.

If the net reverse shock is in the region of the HEM-ISM band near the heavy element ball band, the late part of the net reverse shock is in the heavy element ball band. In the heavy element ball band, there is very few HEM-ISM. Thus, no detectable HEM-ISM emission occurs in the late part of the net reverse shock. The peak of the net forward shock is likely buried in the heavy element ball band as shown in the observation [65]. It is categorized as the “flattening:” type without the peak for the net forward shock. If the net reverse shock appears in the heavy element ball band, no HEM emission by the net reverse shock occurs, resulting in the absence of the prompt afterglow [65].

The length of the ball bands and the length of the effective free relativistic lepton composite jets determine the location of the reverse shock. They relate to Poynting flux and the kinetic energy in the relativistic balls, respectively in the fireball model [65]. The strong reverse shock emission requires the location of the reverse shock in the high-density area of the HEM-ISM band and far away from the heavy element ball band.

When the neutron balls enter the HEM-ISM band, they decay, and leave trails of hydrogen. The trail of hydrogen becomes the factory for amino acid. Hydrogen reacts with carbon, nitrogen, and oxygen to form methane, ammonia, and water, respectively. The combination of photon, hydrogen, methane, ammonia, and water forms amino acids as in the 1950 experiment by Stanley Miller. The highly polarized light during the GRB provides the chirality for the formation of handed amino acids. The heavy element balls trap and carry the amino acids. Many billion years after, one of them provides the source of life on the earth.

A similar volcano eruption in a small scale can take place on a giant magnetar as soft gamma ray repeaters (SGR) [67] [68]. It is the short GRB that lasts less than 2 seconds with much less intrinsic brightness and total emission than the long GRB. A giant magnetar has the LHC remnant and a significant amount of embedded heavy elements. Before a major volcano eruption, the cracks develop under a large embedded heavy element segment. The relativistic lepton composite fills the cracks. Eventually, the relativistic lepton composite breaks the embedded heavy element segment into pieces, and ejects them. The volcano ejects first the small pieces of heavy element as the HEM jets, and then ejects the large pieces as the heavy element balls. A part of the neutron

body is also ejected as the neutron balls. Finally, the volcano ejects the accumulated relativistic lepton composite as the relativistic lepton composite jets. After that, the whole process of the GRB and the afterglow take place.

In summary, the impact of a neutron star on a supermassive gravastar causes cracks, initiating the relativistic lepton composite-powered volcano eruption. The volcano ejects the heavy element materials, the heavy element balls, the neutron balls, and the relativistic lepton composite jets sequentially. The relativistic lepton composite jets accelerate the neutron balls into the relativistic neutron balls, resulting in the GRB. After the GRB, the collisions between the relativistic neutron balls and the non-relativistic balls result in the X-ray afterglow. After the stop of the volcano eruption, the volcano continues to eject the weak residual relativistic lepton composite jets for few days. The combination of the original strong relativistic lepton composite jets during the eruption and the weak residual relativistic lepton composite jets after the eruption brings about the net reverse shock and the net forward shock for the prompt afterglow and the late afterglow, respectively. The short GRB is the small-scale volcano eruption on a giant magnetar.

The long GRB is a rare event. The collisions with the large objects other than neutron stars do not lead to the GRB. They cause the minor volcano eruptions on the gravastar, resulting in the supernova-like emissions, which are not observable from large cosmological distances. The supermassive gravastar is likely at the center of galaxy. In the early universe, the collision between the gravastar and a neutron star or other large objects occurred often, resulting in high frequency of the gravastar volcano eruption. Such high frequency of the gravastar volcano eruption is a major power source of quasars. Quasars are believed to be the most remote objects in the universe. The earliest quasars detected so far are about 700 millions years after the big bang. The closest quasars detected so far are about 800 millions light years away. Despite their small size they produce tremendous amounts of light and microwave radiation. The power source of quasars is not much bigger than the solar system, but they pour out 100 to 1,000 times as much light as a typical galaxy containing a hundred billion stars. A major power source of quasars is from the repetitive gravastar volcano eruptions.

#### 4.4 Summary

Under extreme conditions, such as the zero temperature and extremely high pressure, the extreme force fields as extreme boson force fields form. The formation of the extreme molecule (the Cooper pair) and the extreme lattice provides the mechanism for the phase transition to superconductivity, while the formation of extreme atom with electron-extreme boson provides the mechanism for the phase transition to the fractional quantum Hall effect. The formation of the extreme gluon force field provides the mechanism for the phase transition to gravastar from a collapsing star. Gravastar consists of the lepton composite-extreme gluon force field core and the matter shell. Unlike black holes, gravastars continue to appear as neutron stars and the sources for gamma ray bursts. Neutron star is a remnant gravastar after the explosion (supernova) of a large gravastar. A supermassive gravastar with cracks undergoes the “volcano eruption” as gamma ray bursts.

## 5. Summary

In the cosmic organism theory of physics, the universes and the physical laws are changeable, and they are the variable expressions of the cosmic code, as the biological organs of an organism are the variable expressions of the genetic code. The cosmic organism of physics is the theory of everything to explain fully cosmology, dark energy, dark matter, baryonic matter, quantum mechanics, elementary particles, force fields, galaxy formation, and unusual extreme forces. The cosmic organism theory is divided into five parts: the three physical principles, cosmology, the periodic table of elementary particles, the galaxy formation, and the extreme force field. The cosmic code consists of the three physical principles: the object structure, the space structure, and the dimensional oscillation. The object structure consists of 11D membrane ( $3_{11}$ ), 10D string ( $2_{10}$ ), variable D particle ( $1_{\leq 10}$ ), and empty object (0). The space structure includes attachment space (1) and detachment space (0). Relating to rest mass, attachment space attaches to object permanently with zero speed or reversibly at the speed of light. Relating to kinetic energy, detachment space irreversibly detaches from the object at the speed of light. The combination of attachment space and detachment space brings about three different space structures: miscible space, binary lattice space, and binary partition space for special relativity, quantum mechanics, and the extreme force fields, respectively. The dimensional oscillation involves the oscillation between high dimensional space-time with high vacuum energy and low dimensional space-time with low vacuum energy. Our observable universe with 4D space-time has zero vacuum energy.

In terms of cosmology, our universe starts with the 11-dimensional membrane universe followed by the 10-dimensional string universe and then by the 10-dimensional particle universe, and ends with the asymmetrical dual universe with variable dimensional particle and 4-dimensional particles. Such 4-stage cosmology accounts for the origins of the four force fields. The unified theory places all elementary particles in the periodic table of elementary particles with the calculated masses in good agreement with the observed values.

The inhomogeneous structures, such as galaxy, is derived from the incompatibility between baryonic matter and dark matter, like the inhomogeneous structure formed by the incompatibility between oil and water. Cosmic radiation allows dark matter and baryonic matter to be compatible. As the universe expanded, the decreasing density of cosmic radiation increased the incompatibility, resulting in increasing inhomogeneous structures. The five stages of the formation of inhomogeneous structures are baryonic matter, baryonic droplets, the first generation galaxies by the big eruption, cluster, and supercluster. The big eruption explains the origin of different types of galaxies.

Under extreme conditions, such as the zero temperature and extremely high pressure, gauge boson force field undergoes the phase transition to form extreme force field. Extreme force field explains unusual phenomena such as superconductor, fractional quantum Hall effect, supernova, neutron star, gamma ray burst, and quasar.

## 6. Reference

Email address: [einsnewt@yahoo.com](mailto:einsnewt@yahoo.com)  
Website (download all books): <http://sites.google.com/site/einsnewt/>  
Books list: <http://www.scribd.com/people/documents/1450570-einsnewt>

- 
- [1] D. Chung and V. Krasnoholovets, The Cosmic Organism Theory, Scientific Inquiry 8 (2007), 165-182, <http://www.iigss.net/Scientific-Inquiry/Dec07/3-krasnoholovets.pdf>, arXiv: physics/0512026, [http://arxiv.org/PS\\_cache/physics/pdf/0512/0512026v1.pdf](http://arxiv.org/PS_cache/physics/pdf/0512/0512026v1.pdf)
  - [2] D. Chung,, The Unified Theory of Physics, arXiv:hep-th/0201115, <http://arxiv.org/ftp/hep-th/papers/0201/0201115.pdf>
  - [3] V. Krasnoholovets, and D. Y. Chung, The Space Structure, Force Fields and Quantum Mechanics,, International Journal of Anticipatory Computing Systems (2006), ed. by D. Dubois, 191-197, [http://inerton.org/Inerton\\_Theory\\_-\\_Papers\\_-\\_Sub-microscopic\\_Mechanics\\_files/30\\_Chung&Krasn\\_1.pdf](http://inerton.org/Inerton_Theory_-_Papers_-_Sub-microscopic_Mechanics_files/30_Chung&Krasn_1.pdf)
  - [4] D. Chung, D. and V. Krasnoholovets, V., The Quantum Space Phase Transitions for Particles and Force Fields, Progress in Physics 4 (2006) 74, [http://www.ptep-online.com/index\\_files/2006/PP-06-14.PDF](http://www.ptep-online.com/index_files/2006/PP-06-14.PDF)
  - [5] B. M. Diaz and P. Rowlands, American Institute of Physics Proceedings of the International Conference of Computing Anticipatory Systems (2003), ed. Daniel Dubois
  - [6] J. S. Bell, Physics 1 (1964), 195
  - [7] R. Penrose, Mathematical Physics (2000) eds: by A. Fokas, A. Grigoryan, T. Kibble & B. Zegarlinski (Imperial College, London), pp. 266-282.
  - [8] A. H. Guth, Phys. Rev. D 23 (1981) 347
  - [9] A. Vilenkin, Phys. Rev. D 27 (1983) 2848
  - [10] A. Linde, A. Phys Lett B175 (1986) 395
  - [11] J. Moffat, Int. J. Mod. Phys. D2 (1993)351 [arXiv: gr-qc/9211020]
  - [12] A. Albrecht and J. Magueijo, Phys.Rev. D59 (1999) 043516 [arXiv: hep-ph/9811018]
  - [13] J. D. Barrow, Phys. Lett. B564 (2003) 1, [arXiv: gr-qc/0211074]
  - [14] T. R. Mongan, General Relativity and Gravitation 33 (2001) 1415 [arXiv: gr-qc/0103021]; General Relativity and Gravitation 37 (2005) 967 [arXiv: gr-qc/0501014]
  - [15] J. D. Barrow, G. F. R. Ellis, R. Maartens, and C. G. Tsagas, Class Quantum Grav. 20 (2003), L155 [arXiv: gr-qc/0302094]
  - [16] L. Randall and R. Sundrum, Phys.Rev.Lett. 83 (1999) 4690 [arXiv: hep-th/9906064]
  - [17] M. Bounias and V. Krasnoholovets, The Int. J. Systems and Cybernetics 32, (2003) 1005-1020 [arXiv: physics/0301049]
  - [18] J. Maldacena, Adv. Theor. Math. Phys. V. 2 (1998) 231 [arXiv: hep-th/9711200]
  - [19] S. S. Gubser, I. R. Klebanov, and A. M. Polyakov, Phys. Lett.B v. 428 (1998) 105 [arXiv: hep-th/9802109]
  - [20] E. Witten, Adv. Theor. Math. Phys. V. 2 (1998) 253 [arXiv: hep-th/9802150]
  - [21] P. J. Steinhardt and N. Turok, Phys.Rev. D65 (2002) 126003 [arXiv: hep-th/0111098]
  - [22] J. Khoury, Invited talk at the 6th RESCEU Symposium, 2003, [arXiv: astro-ph/0401579]
  - [23] R. M. Santilli, "Isodual theory of antimatter with applications to antigravity, grand unification, and cosmology" (Kluwer Academic Publishers, Boston/Dordrecht/London) 2006.
  - [24] T. Padmanabhan, Phys. Rept. 380 (2003) 235
  - [25] M. Bounias and V. Krasnoholovets, The Int. J. Systems and Cybernetics 32, no. 7/8, (2003) 945-975 [arXiv: physics/0211096]
  - [26] C. L. Bennett et al, Astrophys.J.Suppl. 148 (2003) 1, [arXiv: astro-ph/0302207]
  - [27] B. Feng, X. L. Wang and X. Zhang, Phys. Lett. B607 (2005) 35.
  - [28] Z.K. Guo, Y.S. Piao, X. Zhang and Y.Z. Zhang, Phys. Lett. B608 (2005) 177.
  - [29] M. Li, B. Feng and X. Zhang, JCAP 0512 (2005) 002.
  - [30] Y. F. Cai, T. Qiu, Y. S. Piao, M. Li and X. Zhang, JHEP 0710, 071 (2007) [arXiv: gr-qc/07041090].

- 
- [31] Y. F. Cai, T. Qiu., R. Brandenberger, Y. S. Piao, and X. Zhang, arXiv: hep-th/ 07112187
- [32] D. Chung, *Speculations in Science and Technology* 20 (1997) 259 [arXiv: hep-th/0111147]
- [33] Particle data Group, (2004)  $\sin^2 \theta_w = 0.2397$
- [34] A.O. Barut, *Phys. Rev. Lett.* 42(1979) 1251; A. Gsponer and J. Hurni, arXiv: hep-ph/0201193
- [35] P. Langacher, M. Luo , and A. Mann, *Rev. Mod. Phys.* 64 (1992) 87
- [36] L. Hall, R. Jaffe, J. Rosen, *Phys. Rep.* 125 (1985) 105
- [37] C.P. Singh, *Phys. Rev. D*24 (1981) 2481; D. B. Lichtenberg *Phys. Rev. D*40 (1989) 3675
- [38] Particle data Group, (2004)
- [39] K. Miuchi et al, *Astropart. Phys.* 19, 135 (2003) [arXiv: astro-ph/ 0204411]; CDMS Collaboration, *Phys.Rev. D*68, 082002 (2003) [arXiv: hep-ex/0306001]
- [40] M. Milgrom, *New Astron.Rev.* 46 (2002) 741-753 [arXiv: astro-ph/0207231], astro-ph/0112069; R. H. Sanders and S. McGaugh arXiv: astro-ph/0204521
- [41]D. Chung, *The Evolution of Galaxies by the Incompatibility between Dark Matter and Baryonic Matter*, arXiv: hep-th/0112036, <http://arxiv.org/ftp/hep-th/papers/0112/0112036.pdf>
- [42] A. H. Guth, *Phys. Rev. D* 23, 347 (1981), A. D. Linde, *Phys. Lett.* B108 (1982) 389; A. Albrecht and P. J. Steinhardt, *Phys. Rev. Lett.* 48 (1982) 1220
- [43] A. C. S. Readhead et al astro-ph/0402359; Rafael Rebolo et al astro-ph/0402466
- [44] A. Dekel, Y. Birnboim, G. Engel, J. Freundlich, T. Goerdt, M. Mumcuoglu, E. Neistein, C. Pichon, R. Teysier, E. Zinger, *Cold streams in early massive hot haloes as the main mode of galaxy formation*, arXiv:astro-ph/0808.0553, *Nature*, 457, 451-454, 2009.
- [45] R. Barkana and A. Loeb, arXiv: astro-ph/0209515
- [46] B. M. Tinsley and J. E. Gunn *ApJ* 203 (1976) 52
- [47] C. Conselice, arXiv: astro-ph/0212219
- [48] B. M. Poggianti, astro-ph/0210233, S. F. Helsdon and T. J. Ponman, arXiv: astro-ph/0212047
- [49] S. Leon, J. Braine, P. Duc, V. Charmandaris, and E. Brinks, astro-ph/0208494, arXiv: astro-ph/0210014
- [50] M. Bonamente, M. Joy, and R. Liu, arXiv: astro-ph/0211439
- [51] J. Einasto, G. Hutsi, M. Einasto, E. Saar, D. L. Tucher, V. Muller, P. Heinamaki, and S. S. Allam, arXiv: astro-ph/0212312
- [52] M. J. West, astro-ph/9709289
- [53] P. Coleman and A. Schofield, *Nature* 433 (2005) 226
- [54] P. W. Anderson, P. A. Lee, M. Randeria, T. M. Rice, N. Trivedi, and F. C. Zhang *Phys.: Condens. Matter* 16 (2004) R755-R769, cond-mat/0311467
- [55] A. Ramsak and P. Prelovsek, *P. Proc. of SPIE* (2005) 59320G-2, cond-mat/0506726
- [56] D. C. Tsui, H. L. Störmer, and A. C. Gossard, *Phys. Rev. Lett.* 48 (1982) 1559-1562
- [57] R. B. Laughlin, *Phys. Rev. Lett.* 50 (1983) pp 1395-1398
- [58] J. K. Jain, *Phys. Rev. Lett.* 63 (1989) pp. 199-202
- [59] H. Stormer, *Physica B* 177 (1992) pp. 401-408.
- [60] P. O. Mazur and E. Mottola, “Gravitational condensate stars: An alternative to black holes”, preprint LA-UR-01-5067 (2001) [arXiv: gr-qc/0109035]
- [61] P. O. Mazur and E. Mottola, *Proc. Nat. Acad. Sci.* 111 (2004) pp. 9545-9550 [arXiv: gr-qc/0407075]
- [62] G. Chapline, *Proceedings of the Texas Conference on Relativistic Astrophysics*, Stanford, CA, December, 2004 [arXiv: astro-ph/0503200]
- [63] H. A. Bethe, *Rev. Mod. Phys.* 62 (1990), pp. 801-866
- [64] B. Zhang and P. Mészáros, *Int. J. Mod. Phys. A* 19 (2004) pp. 2385-2472 (arXiv:astro-ph/0311321)
- [65] T. Piran, , *Rev. Mod. Phys.* 76 (2005), pp. 1143-1210 [arXiv: astro-ph/0405503]
- [66] B. Zhang, *Proc. of "Astrophysics Sources of High Energy Particles and Radiation"* (eds. T. Bulik, G. Madejski and B. Rudak), Torun, Poland, 20-24 June, 2005 [arXiv: astro-ph/0509571]
- [67] E. Nakar, T. Piran, and R. Sari, *Astrophys. J.* 635 (2005) 516 [arXiv: astro-ph/0502052]
- [68] A. Dar, *Chin. J.Astron.Astrophys.* 6 (2006) 323 [arXiv: astro-ph/0509257]